SMYD5 is a novel epigenetic gatekeeper of the mild hypothermia response

Salvor Rafnsdottir[1], Kijin Jang[1], Sara Tholl Halldorsdottir[1], Arnhildur Tomasdottir[1], Meghna Vinod[1], Katrin Möller[1], Tinna Reynisdottir[1], Laufey Halla Atladottir[1], Kristin Elisabet Allison[2], Jin He[3], Li Zhang[4], Frances J. Northington[5], Raul Chavez-Valdez[5], Kimberley Jade Anderson[1], Hans Tomas Bjornsson[1,4,6,7*]

[1]Louma G. Laboratory of Epigenetic Research, Faculty of Medicine, University of Iceland, Reykjavik, Iceland; [2]Faculty of Life and Environmental Sciences, University of Iceland, Reykjavik, Iceland; [3]Department of Biochemistry and Molecular Biology, College of Natural Science, Michigan State University, MI, USA; [4]McKusick-Nathans Department of Genetic Medicine, Johns Hopkins University School of Medicine, MD, USA; [5]Division of Neonatology, Department of Pediatrics, Johns Hopkins University School of Medicine, Baltimore, MD, USA; [6]Department of Pediatrics, Johns Hopkins University, MD, USA; [7]Department of Genetics and Molecular Medicine, Landspitali University Hospital, Reykjavik, Iceland.

***Corresponding author:** Hans Tomas Bjornsson, htb@hi.is

Summary

Organisms have homeostatic mechanisms to respond to cold to ensure survival including the activation of the neuroprotective mild hypothermia response (MHR) in mammals at 32°C. We show activation of the MHR by one FDA-approved medication, Entacapone, a proof-of-principle that the MHR can be medically manipulated. Utilizing a forward CRISPR-Cas9 mutagenesis screen, we identify the histone lysine methyltransferase SMYD5 as an epigenetic gatekeeper of the MHR. SMYD5 represses the key MHR gene *SP1* at euthermia but not at 32°C. This repression is mirrored by temperature-dependent levels of H3K36me3 at the *SP1*-locus and globally indicating the mammalian MHR is regulated at the level of histone modifications. We identified 45 additional SMYD5-temperature dependent genes suggesting a broader MHR-related role for SMYD5. Our study provides an example of how the epigenetic machinery integrates environmental cues into the genetic circuitry of mammalian cells and suggests novel therapeutic avenues for neuroprotection after catastrophic events.

Keywords: Targeted Temperature Management, SP1, Hypothermia, Neonatal asphyxia, cardiac arrest

31 **Visual abstract**

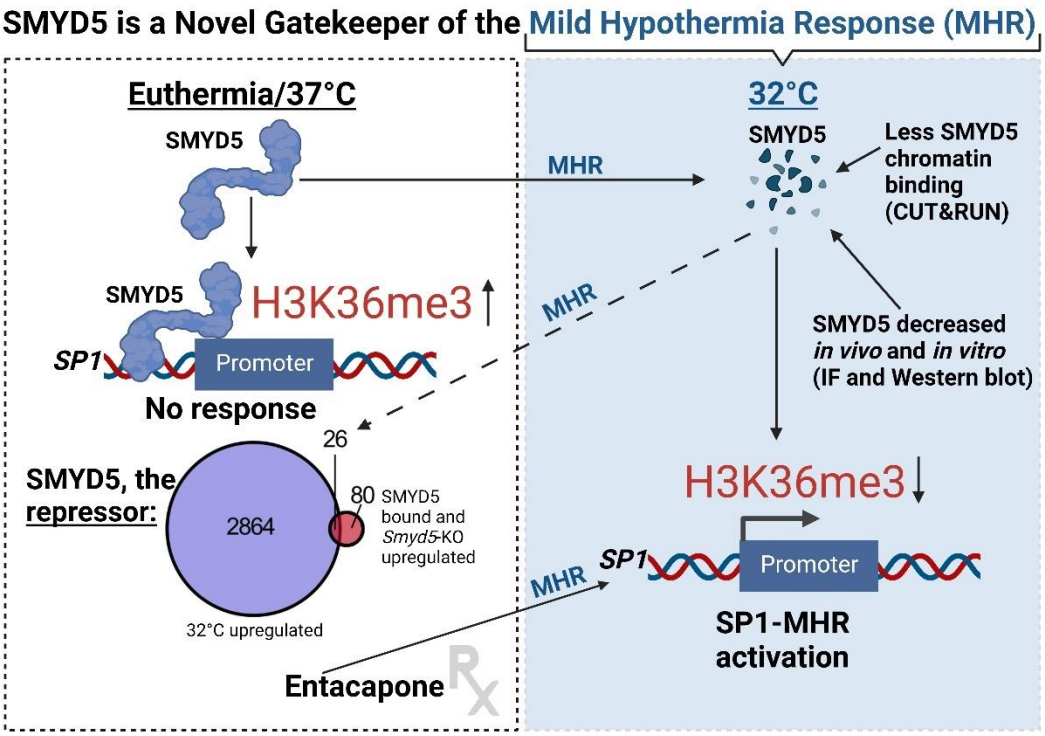

32

33 **Introduction**

34 The defining feature of mammals is their ability to maintain an elevated body temperature
35 and most maintain a relatively tight range to ensure normal cellular homeostasis[1]. The main
36 exception is hibernation of some mammals, which is a type of controlled decrease of temperature
37 during times of prolonged inactivity[2]. In clinical practice, physicians imitate hibernation with the use
38 of Targeted Temperature Management (TTM) as a therapeutic strategy to minimize neurological
39 damage following neonatal asphyxia and cardiac arrest[3,4]. The reasons why lowered internal core
40 temperature (32°C-36°C) yields benefits are currently not fully understood[5,6]. Although some argue
41 that the positive neurological benefit from mild hypothermia relates to lower metabolic rate, others
42 point out that the specific upregulation of several genes during mild hypothermia does not fit that
43 idea[7]. An obvious alternative hypothesis is that hypothermia is beneficial, because of the activation
44 of the mild hypothermia response (MHR) itself and if so, it would be important for researchers and
45 clinicians to understand the extent of the response. In support of this, researchers have found that
46 several genes (e.g., *CIRBP/CIRP*, *RBM3*) consistently show increased expression during mild
47 hypothermia[8]; two of these, *SP1* and *RBM3,* appear to have roles in decreasing neuronal death
48 during disease states[9–13].

49 Scientists have recently found that SP1, a transcription factor known to bind at the promoter
50 of many genes[14], binds to the promoter region of *CIRBP*[15] upon cold exposure at a sequence called
51 the Mild Cold Response Element (MCRE)[15], and its binding leads to increased expression of *CIRBP* at
52 32°C, indicating that this regulation occurs at the transcriptional level[15]. Similarly, RBM3 is known to
53 regulate at least one down-stream gene, *RTN3*[11], a potential neuroprotective factor in a
54 neurodegeneration model[11]. Although this suggests that mammalian cells have a pathway
55 culminating in SP1/CIRBP and RBM3/RTN3, little has been done to further elucidate the upstream
56 regulation of this pathway and relatively little knowledge is available regarding mammalian cellular
57 responses to cooling compared to heat shock responses, which have been previously extensively
58 characterized[16].

59 Here, we use complementary and unbiased strategies to gain clues into the MHR upstream
60 of *SP1*. Specifically, we use a novel *SP1* mild hypothermia indicator (MHI) containing the MCRE
61 enhancer (SP1+MCRE-MHI) to perform compound screening of 1953 FDA-approved agents. We
62 successfully validated the drug Entacapone that activates the endogenous MHR at the transcriptional
63 level; this indicates that it is possible to manipulate the response without exposure to hypothermia.
64 To identify additional gene regulators, we performed a genome-wide CRISPR-Cas9 forward
65 mutagenesis screen[17–19], reading out *SP1*-promoter activity using the SP1-MHI. Our study yielded

66 multiple candidate regulators and compounds that may regulate the MHR. We focus on one of these
67 regulators, *SMYD5*, a histone methyltransferase, and demonstrate that the presence of SMYD5 is
68 temperature dependent and that a number of other SMYD5-bound genes show significant
69 differential expression upon mild hypothermia exposure. Our insights elucidate how an external cue
70 (mild hypothermia) specifically mediates its effects on the human genome through the actions of the
71 epigenetic machinery. These results paves the way towards the development of a novel therapeutic
72 means to treat asphyxia, a major cause of mortality and morbidity in otherwise healthy newborns[20].

73 **Results**

74 Mild hypothermia indicators show increased fluorescence at mild hypothermia (32°C).

75 Core temperature (euthermia) is kept at a very tight range in humans (36,5-37,8°C)[1,21] and by
76 definition mild hypothermia involves temperature ranging from 32-36°C (**Figure S1**, **bold**). In order to
77 directly visualize the promoter activity of three genes previously shown[8] to respond to mild
78 hypothermia (*CIRBP*, *RBM3*, *SP1*), we made eight distinct MHIs (**Supplementary table 1;**
79 **Supplementary file 1**) all of which have promoter and/or MCRE sequences, driving the expression of
80 either GFP or mCherry (**Figure 1A**). When transfected into HEK293 cells, the MHIs demonstrate
81 increased fluorescence at 32°C compared to 37°C (**Figure 1B–1C)**. These findings are mirrored by
82 endogenous SP1 levels in a Western blot from cells collected after 16 hours at 32°C (h, **Figure 1D**).
83 We assessed the temporal dynamics of promoter activity using flow cytometry analysis of the three
84 indicators and observed a maximal increase in fluorescence of SP1-MHI between 6-8 h after a
85 temperature shift to 32°C ($P<0.05$, **Figure 1E**). This finding was supported by a separate method
86 (continuous monitoring of fluorescence from a Incucyte S3), again maximal intensity was reached
87 within 6-8 h, with SP1-MHI, rising fastest, followed by RBM3-MHI, and then CIRBP-MHI (**Figure S2A-**
88 **S2C**). Indicators were also transiently transfected into HEK293 cells and then exposed to five distinct
89 temperatures (26°C, 29°C, 32°C, 37°C and 40°C), for 16 h followed by flow cytometry **(Figure 1F-1H;**
90 **Figure S2D-S2E**). Consistent with previous literature[8,15], and our own validation in HEK293 cells
91 (**Figure 1C**), indicators representing all three genes (*SP1*, *CIRBP*, *RBM3)* had significantly ($P<0.0001$)
92 increased fluorescence at 32°C compared to 37°C/40°C (**Figure 1F-1H**) and the response was
93 uniformly strongest at 32°C (**Figure 1F-1H**). At the same time, the SP1- and CIRBP-MHIs do not show
94 increased activity at lower (26°C, 29°C, **Figure S2D-S2E**) or higher (40°C) temperatures (**Figure 1F-1G**),
95 supporting the notion that our MHIs specifically reflect the MHR and are not activated by general cell
96 stress (i.e., heat stress or moderate hypothermia). These data suggest that all three genes are
97 regulated at the transcriptional level and the time-lag in the response upon hypothermia, measured
98 in hours rather than minutes, indicates that there must be additional regulators operating upstream
99 of these genes. Some would argue that storing cells on ice (i.e., during fluorescent activating cell

sorting (FACS)) could possibly lower the temperature of cells to the hypothermic range and activate the MHR, but we found that even prolonged storage on ice (8 h) was unable to activate the MHI (**Figure S3A-S3D**), ensuring that storage on ice during the study could not act as a potential confounder.

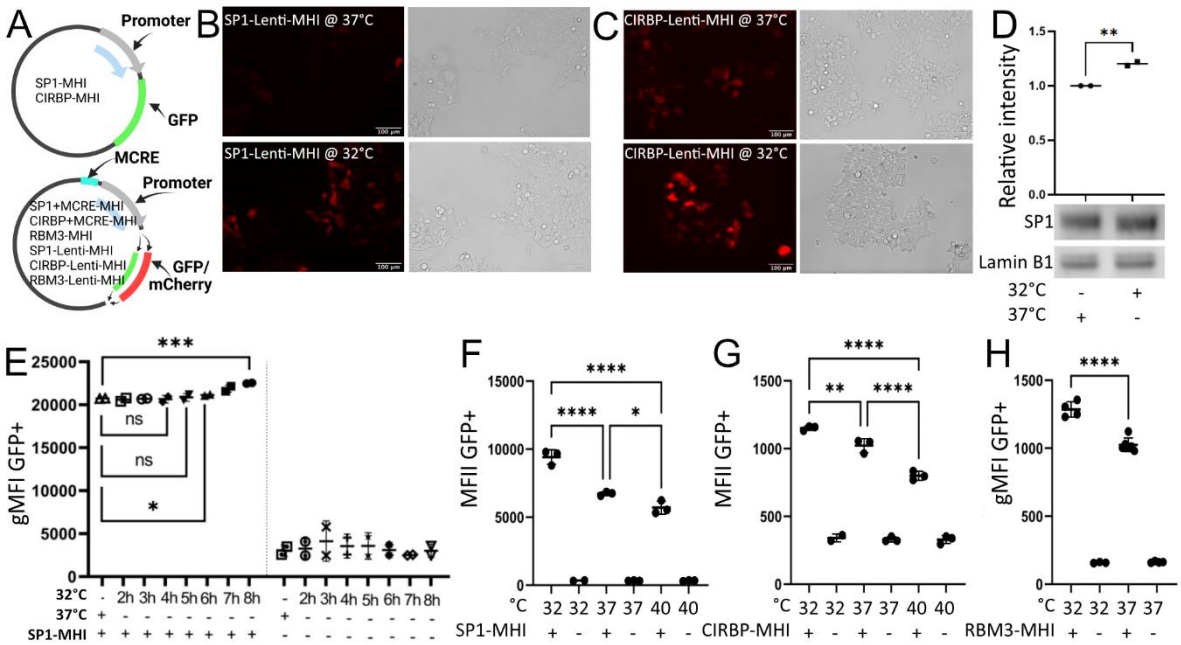

Figure 1. MHIs based on all three genes (*SP1*, *CIRBP*, *RBM3*) show strongest effect at 32°C. (A) A schematic of MHI structures. (B-C) Representative images of SP1-Lenti-MHIs and CIRBP-Lenti-MHI, respectively, at 37°C and 32°C as visualized by fluorescent microscope. (D) Western blot quantification demonstrating increased SP1 after 16 h at 32°C compared to 37°C. Shown are data points, each data point is a biological replicate, mean and SD where applicable. Significance levels were calculated with an unpaired one-tailed t-test in GraphPad Prism. (E) Geometric mean fluorescence (gMFI, flow cytometry) at different timing of hypothermia exposure for SP1-MHI. Each data point is a technical replicate. (F-G) Mean fluorescence (MFI, flow cytometry) of SP1-MHI and CIRBP-MHI (16 h at 32°C, 37°C, 40°C), respectively. Shown are data points, each point is a technical replicate, mean and SD where applicable. Significance levels were calculated in GraphPad Prism with Šidák's multiple comparison test. (H) gMFI of RBM3-MHI (16 h at 32°C and 37°C). Significance level were calculated with unpaired one-tailed t-test in GraphPad Prism otherwise data shown as in (G-H). * = P<0.05, ** = P<0.01, *** = P<0.001, **** = P<0.0001.

Activation of the MHR at 32°C is uniformly seen in cells of diverse origins.

In addition to HEK293 cells, which has been widely used in prior studies[11,15,22], we sought to verify that our novel MHIs also work in diverse cellular systems. We transiently transfected three individual MHIs (SP1-, RBM3-, SP1+MCRE-MHI) into six distinct cell lines: (HEK293, HCT-116, HeLa, Jurkat, K562 and SK-N-SH), representing diverse cellular origins including embryonic kidney, colon, cervix, T lymphocytes, lymphoblasts and neurons, respectively. After exposing these cells to 26°C,

125 29°C, 32°C, 37°C and 40°C for 16 h and quantifying the fluorescence by flow cytometry, we observed
126 highest fluorescence at 32°C independent of cellular origin (**Figure S4**) and no effect for moderate
127 hypothermia (26-29°C, **Figure S5, Figure S2E-S2F**) with the exception of SK-N-SH and K562 cell lines
128 (**Figure S5D-S5E**). The strongest activation of MHI at 32°C was detected in the cell-types previously
129 described to have neurological characteristics (HEK293 and SK-N-SH)[23–25] and these were also the cell
130 lines that showed significant activation of all three MHIs at 32°C (**Figure 1F-1H; Figure S4**). This is
131 consistent with prior literature showing that the RBM3-MHR response is strongest in young
132 neurons[26]. Since many of the key studies in the field have used HEK293 [11,15,22] and they have neuronal
133 characteristics[23,25] we used this cell line for experiments going forward.

134

135 Compound screening reveals MHR activators at euthermia.

136 In our search for therapeutic targets for TTM, we sought to identify compounds that could
137 activate the MHR at 37°C as this could yield insights into the involved biochemical pathways. To
138 explore this in an unbiased manner, we performed a systematic library drug screen (1953 FDA-
139 approved inhibitors, **Figure 2A**) using HEK293T cells transfected with the SP1+MCRE-MHI. Cells
140 transfected with SP1+MCRE-MHI were exposed to the drugs (20 µM concentration) and fluorescence
141 was measured after 16, 28 and 40 h of drug exposure (**Figure 2A**). We focused on drugs that increase
142 the MHI fluorescence at least ≥3.75 times at one of the time points (**Supplementary Table 2**). Among
143 these drugs we saw an apparent albeit non-significant enrichment of Tyrosine Kinase Inhibitors (TKI,
144 7/80, $p<0.075$) including Orantinib, Dasatinib (hydrochloride, monohydrate), Poziotinib, Rociletinib,
145 Afatinib, and Lapatinib[27–31]. We validated three from this group (Dasatinib, Orantinib, and Pozitinib)
146 as well as selecting another 5 drugs that showed one of the greatest responses in the screen
147 (Cinacalcet, Entacapone, Erythromycin, Naloxone, and Tamoxifen, **Figure 2B**). For validation of the
148 drug screen HEK293 cells expressing SP1-MHI were individually exposed to each of the 8 compounds
149 (20 µM) for 16 h at either 32°C or 37°C followed by flow cytometry. Two out of the eight (25%),
150 showed significantly ($P<0.001$, $P<0.0001$) increased fluorescence at 37°C (Entacapone, Poziotinib,
151 **Figure 2C-2D**), indicating these two drugs can potentially induce the MHR. Entacapone also had
152 significantly ($P<0.01$) enhanced fluorescence levels at 32°C (**Figure 2C**), suggesting that the effect is
153 additive and thus synergistic to the regular response and thus likely independent of the SP1 target
154 itself. Other compounds did not increase the fluorescence of the SP1-MHI for the dose tested (**Figure**
155 **S6A-S6F**). To exclude the possibility of cell cycle arrest or increased apoptosis[31,32], we evaluated the
156 cell cycle phase in HEK293 cells exposed to Poziotinib and Entacapone and no apparent signs of cell
157 cycle arrest were observed for either compound, other than a slight increase in the percentage of
158 total cells in the S phase of the cell cycle after Entacapone exposure (**Figure S6G**). After exposing

159 HEK293 cells to the apoptotic agent H_2O_2 we could not see any signs of activation of the SP1-MHI
160 (**Figure S6H**), but we observed a significant (P<0.01) increase of fluorescence after only 4 h at 32°C
161 (**Figure S6H**) suggesting that cell stress may potentiate the response. To our surprise, three drugs
162 (Cinacalcet, Dasatinib, and Tamoxifen) showed significantly decreased fluorescence of the SP1-MHI
163 at 32°C during this validation (**Figure S6A, S6B and S6F**). To evaluate the endogenous effects on SP1
164 we carried out Western blotting after 24 h exposure to the compounds at either 32°C or 37°C. For
165 Entacapone (20 µM concentration) we observed a significant increase of SP1 at 37°C (P<0.05**, Figure**
166 **2F**). We were unable to test Poziotinib at 20 µM due to low protein yields therefore we performed
167 the western blot at a lower dose (4 µM) and for this dose we only saw a trend towards increased SP1
168 at 37°C (**Figure 2G**). When we looked at mRNA levels for *SP1*, *CIRBP* and *RBM3* at 32°C and 37°C after
169 16 h of Entacapone and Poziotinib exposure (20 µM), we only observed a significant (P<0.01)
170 elevated *RBM3* mRNA levels upon Poziotinib exposure at 37°C (**Figure S7**). This could suggest that the
171 drugs may impact both transcriptional and post-transcriptional levels of key factors of the MHR.

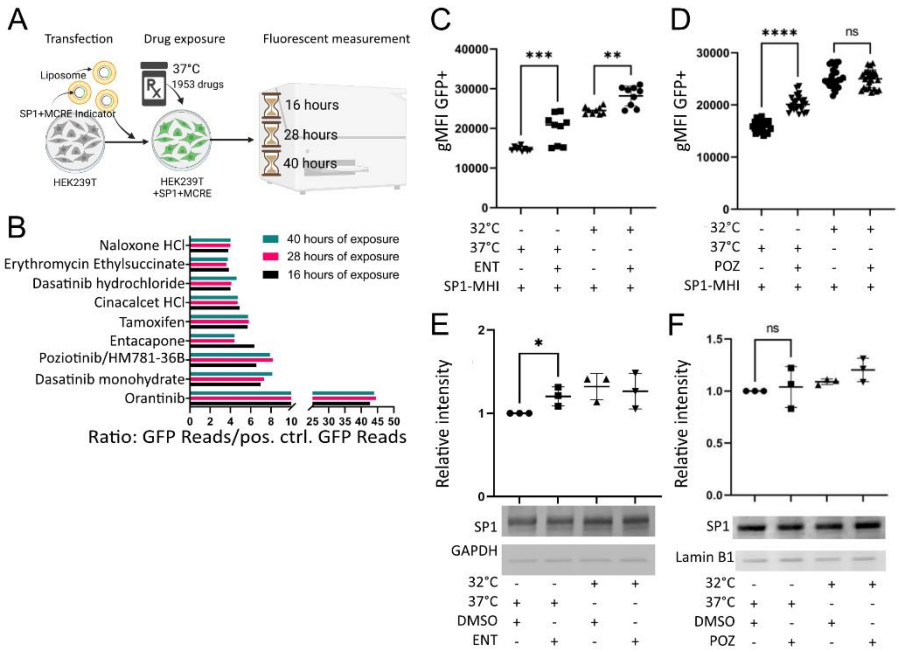

172

173 **Figure 2. Poziotinib and Entacapone activate the MHR.** (A) A schematic overview of our drug screen
174 in HEK293T cells transfected with SP1+MCRE-MHI. (B) Representative drugs were found to cause
175 more than ≥3.75 times increase of SP1+MCRE-MHI fluorescence. The entire list is provided as
176 **Supplementary Table 2**. (C-D) gMFI of SP1-MHI as measured by flow cytometry after 16 h of either
177 32°C or 37°C with or without Entacapone (ENT, C, 20 µM) and Poziotinib (POZ, D, 20 µM) exposure.
178 Shown are data points, each point is a technical replicate, mean and SD where applicable.
179 Significance levels were calculated in GraphPad Prism with Šidák's multiple comparison test.). (E-F)
180 Western blot of SP1 after exposure to Entacapone (ENT, E, 20 µM) and Poziotinib (POZ, F, 4 µM) or
181 vehicle (DMSO) after 24 h. Shown are data points, each data point is a biological replicate, mean and

182 SD where applicable. Significance levels were calculated with unpaired one-tailed t-test in GraphPad
183 Prism. * = P<0.05, ** = P<0.01, *** = P<0.001, **** = P<0.0001.

184

185 CRISPR-Cas9 Knockout Screen with SP1-MHIs reveals candidate regulators.

186 In an effort to map regulators of the cooling response (*SP1*) in an unbiased manner, we used
187 an available genome-coverage lentiGuide-Puro pooled sgRNA library[17–19] in combination with our
188 SP1-MHI to uncover transcriptional regulators of *SP1* during MHR. We chose to use the SP1-MHI, as
189 our prior data indicate that this gene is regulated at the transcriptional level (**Figure 1**) and is the
190 earliest key MHR gene to achieve maximal response at 32°C (**Figure S2A-S2C)**. However, given that it
191 does not reach its maximal response until 6-8h of hypothermia exposure, we hypothesized that there
192 may be unknown regulators of the *SP1* locus that function earlier in the MHR process. We performed
193 the screen on HEK293WT+Cas9 cells expressing SPI-MHI (HEK293WT+Cas9+SP1), transducing the
194 sgRNA library at the rate of 0.3 sgRNA per cell. After puromycin selection and exposure to
195 hypothermia (32°C) for 16 h (to activate the MHR), we sorted out the 5% most and least fluorescent
196 cells (**Figure 3A**) to capture repressors and activators of *SP1*, respectively. We saw a consistent shift
197 towards lower fluorescence for the transduced HEK293WT+Cas9+SP1-MHI (green) compared to the
198 positive control (non-transduced HEK293WT+Cas9+SP1-MHI, grey) (**Figure 3B**). The observation of
199 such a large fluorescent shift of cells (less SP1-MHI fluorescence) at hypothermia suggests the
200 involvement of many sgRNAs and therefore likely many genes are upstream of *SP1*. Furthermore, this
201 suggests that the majority are activators rather than repressors of the SP1 arm of the MHR. We
202 amplified guides for each sorted group as well as the negative control (transduced HEK293WT+Cas9)
203 and performed deep next-generation sequencing of their distribution from sorted and un-sorted
204 fractions (negative control). To identify guides enriched in the sorted populations, we used the
205 MaGeCK pipeline[33] to computationally predict genes with enrichment (**Figure 3C-3D**). We decided to
206 cast a wide net and look at all genes that had a -Log10 (RRA score) > 2.5 to not miss possible
207 regulators (**Supplementary Table 3**). We excluded 21 genes that were seen in lists for both the high
208 (repressor list) and low (activator list) sorts of transduced HEK293+Cas9+SP1-MHI (**Supplementary**
209 **Table 4**), as these may be related to proliferation rather than the MHR itself, and a validation of two
210 of these (*RGS21* and *MALT1*) supported that idea (**Figure S8**). We were left with a list of 495 genes for
211 the SP1-repressors and 61 for SP1-activators – a clear overrepresentation of repressors to activators
212 (**Supplementary Table 3**). Of note, there were two microRNAs on the top list of SP1-repressors and
213 activators (*hsa-mir-4314* and *hsa-mir-6739*) and both are predicted to target SP1 (mirdb.org).

214 Since the ERBB2/HER2 signaling is known to regulate SP1 binding through phosphorylation[34],
215 and is the target of tyrosine kinases inhibitors such as Poziotinib (**Figure S9A**), we looked through

216 both lists and noted that ERK was found on the SP1-repressor list (**Figure S9A**). On the Qiagen ERBB2
217 Pathway (from Qiagen Inguinity Pathways) there are 22 genes upstream of *SP1*, and among those 3
218 were found on the SP1-repressor list (*RAS*, *ERK*, *STAT5*, P<0.02). We also used the Molecular
219 Signature Database (MSigDB) to establish likely pathways from genes that had a -Log10(RRA) score
220 over 0.5 from each screen (**Figure S9B-S9C**) and observe one shared pathway (Pentose Phosphate
221 Pathway (3P)). Of interest there were two categories in the SP1-activator analysis that implicate
222 cytosolic calcium regulation; calcium influx has been shown to be an immediate event in cells
223 exposed to hypothermic stimuli[35]. As we were particularly interested in a possible transcriptional
224 regulator of *SP1*, we annotated our lists and identified 50 (10%) on the SP1-repressor list and 4 (6%)
225 on the SP1-activator list (**Figure 3E**) as transcriptional regulators. Of these, ten (*GATAD2*, *POU4F3*,
226 *ZNF71*, *KAT5*, *ZNF260*, *ANKZF1*, *SMYD5*, *DMRT1*, *TAF13*, *NKX6-2*) had a -Log10(RRA) score above 3,5
227 in either the repressor or activator screen (**Figure 3F**). For a gene from our list to act as a direct
228 repressor or activator for *SP1* we reasoned that direct regulators from the repressor list should have
229 known functions as repressors and genes from the activator list should have known activating
230 functions. Four genes from the list appeared to have opposing functions (*KAT5*, *ZNF260*, *NKX6-2,*
231 *ANKZF1*, **Figure 3F**, not bold)[36–39] leaving six genes (**Figure 3F,** bold)[40–46] on our list. Histone
232 modification has previously been known to dictate temperature-dependent sex determination in
233 reptiles[47] and vernalization in plants[48], and one of these six targets (*SMYD5*), is a histone
234 methyltransferase, known to catalyze H4K20, H3K9 and H3K36 trimethylation[44,45]. Interestingly,
235 *SMYD5* is a known interactor with *KDM6B* in fish[49] and *KDM6B* mediates the previously described
236 epigenetic temperature dependent sex determination switch in reptiles[47]. Also, like CIRBP and RBM3,
237 SMYD5 is a known resident of stress granules[50]. Since SMYD5 histone tail modifications are known
238 and their levels can be measured at its targets we argued that this might be useful for validation
239 purposes. Thus, we decided to further focus our efforts on *SMYD5*.

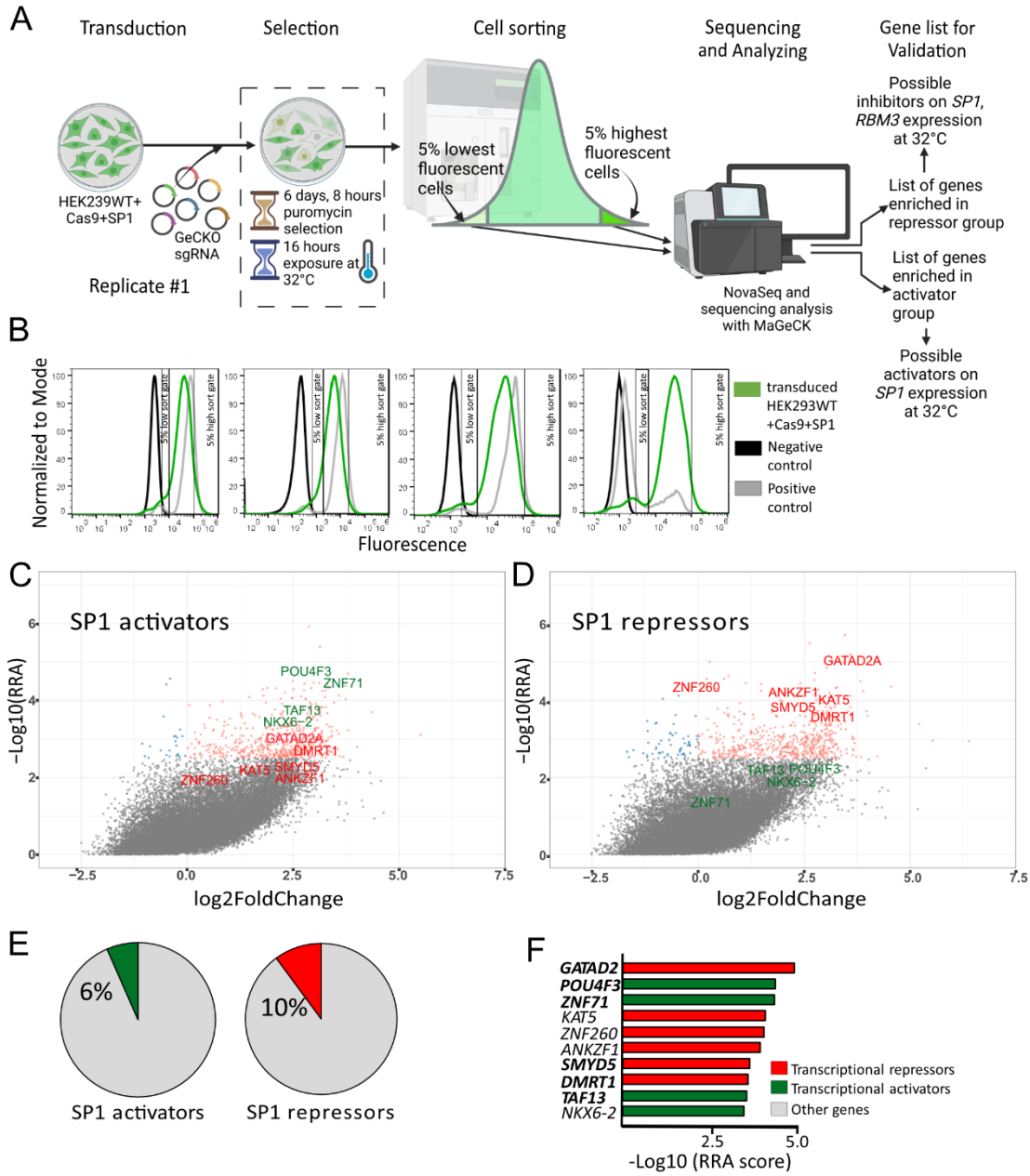

240

241 **Figure 3. Genome wide CRISPR-Cas9 knockout screen on SP1-MHI reveals multiple potential**
242 **inhibitors/activators of the MHR.** (A) Overview over the genome-wide CRISPR-Cas9 Knockout
243 approach for the HEK293WT+Cas9+SP1 cell line. (B) Fluorescence and sort gates of 4 replicates of
244 transduced HEK293WT+Cas9+SP1 cells (green), negative control (HEK293WT, black) and positive
245 control (HEK293WT+Cas9+SP1, grey). (C-D) Genes marked with their name in red are transcription
246 regulators that have -Log10(RRA) score >3.5 and have repressive functions and genes marked with
247 their name in green are transcription regulators that have activating functions and -Log10(RRA) score
248 >3.5. Colored dots represent genes that have -Log10(RRA) score >2.5, where orange dots indicate
249 genes that have positive log fold change (LFC) and blue dots indicate genes that have a negative LFC,
250 from either the SP1 activator (C) or repressor (D) screen. (E) A summary of transcriptional regulators

251 from our screens, activators (green) on left, repressors (red) on right. (F) A summary of top 10
252 transcriptional regulators ranked by their -Log10 (RRA score). Bold genes can act as a direct repressor
253 (red) or direct activator (green).

254

255 SMYD5 is a direct repressor of *SP1*.

256 To further explore the role of SMYD5, we took advantage of a newly published dataset[44]
257 from a CUT&TAG assay in mouse Embryonic Stem Cells (mES) with an overexpressed SMYD5-Flag
258 plasmid. Upon re-analysis of their data, we noticed that SMYD5, has strong peaks at the promoters of
259 both *Sp1* (130K) and *Cirbp (70K),* but not *Rbm3* (**Figure 4A**). These peaks occur at evolutionarily
260 conserved sites and overlap with CpG islands (**Figure 4A**). We took advantage of an RNASeq dataset
261 on *Smyd5* knockout (KO) mESC from the same study[44] and reanalyzed it which yielded approximately
262 equal amounts of upregulated and down-regulated genes among SMYD5 bound loci (**Figure 4B**)
263 supporting prior reports that histone marks deposited by SMYD5 can either repress or activate[44,45].
264 When looking at the three loci (*Sp1*, *Cirbp*, *Rbm3*), we found that *Smyd5*-KO yielded increased
265 expression of *Sp1* but not *Cirbp* or *Rbm3* (**Figure 4C**) suggesting a direct role for SMYD5 as a *Sp1*
266 repressor in a murine system. In this dataset, *Cirbp* showed lower expression compared to *Sp1* and
267 *Rbm3* (**Figure S10**) which may impede interpretation. In order to validate this findings in our own
268 system we decided to knockdown *SMYD5* with siRNA in HEK293WT+Cas9+SP1 cell lines (**Figure 4D**),
269 we observed an increased fluorescence of SP1-MHI at 32°C and 37°C. *SMYD5*-KO with a guide RNA
270 (gRNA) and Cas9 significantly decreased amounts of *SMYD5* mRNA expression by qRT-PCR (**Figure 4E**)
271 and SMYD5 protein levels by Western blot (**Figure 4G**), which are rescued upon overexpression of a
272 gRNA-resistant Flag-SMYD5 plasmid (Flag-SMYD5 sgRNAres plasmid (labelled SMYD5sgRNA#6res),
273 **Figure 4E and 4G**). The same experiment revealed de-repression of the *SP1* transcript in KO cells by
274 RT-qPCR, with repression restored in rescued cells (**Figure 4F**). Furthermore, we observed a
275 significant increase of SP1 and CIRBP, but not RBM3 following *SMYD5*-KO at 37°C using Western blot
276 of the endogenous loci (**Figure 4H-4J**).

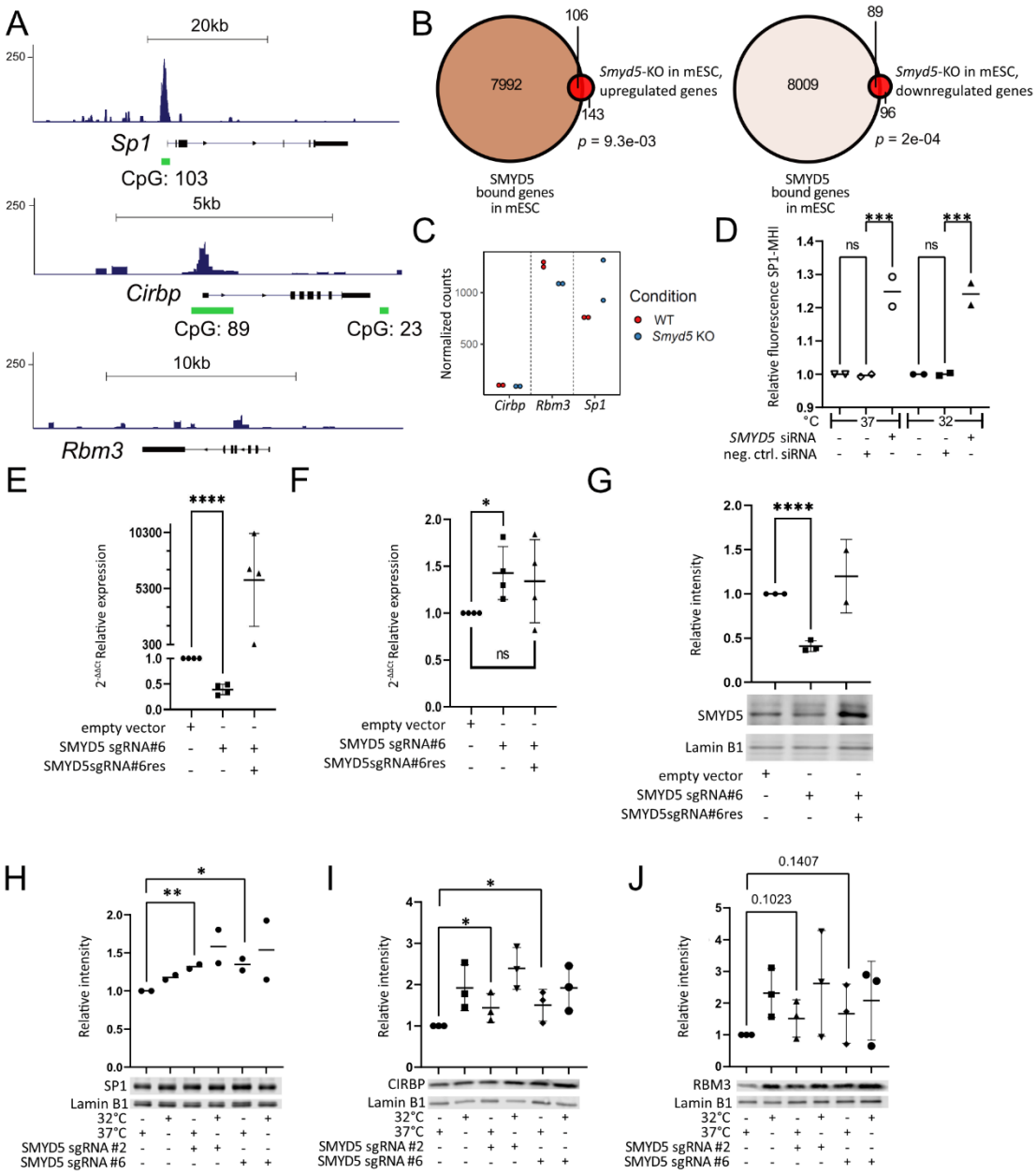

Figure 4. SMYD5 is a repressor of SP1 at 37°C. (A) Overexpressed FLAG-tagged SMYD5 in mESc, binds at promoters of *SP1* and *CIRBP* but not of *RBM3*. (B) Venn graph showing both up- and down-regulated SMYD5-target genes in an RNASeq of *Smyd5*-KO cells. Statistical analysis done with GeneOverlap package in R using Fisher's Exact test. (C) *Smyd5*-KO leads to increased expression of *SP1* but not *RBM3* or *CIRBP* in mESCs. (D) *SMYD5* knockdown by siRNA yields higher levels of fluorescence of SP1-MHI at 32°C and 37°C compared to empty vector control. Shown are data points, each data point is a biological replicate that has been normalized against same non-transfected HEK293WT+Cas9+SP1-MHI cell line and a mean of data points. Significance levels were calculated with Šidák's multiple comparison test in GraphPad Prism. (E) Relative expression of *SMYD5* compared to GAPDH from *SMYD5*-KO cells, measured by RT-qPCR at 37°C, with or without rescue with Flag-SMYD5 sgRNAres plasmid (labelled SMYD5 sgRNA#6res) which demonstrates that SMYD5-KO was

289 successful. Shown are data points, each data point is a biological replicate, mean and SD where
290 applicable. Significance levels were calculated with unpaired one-tailed t-test in GraphPad Prism. (F)
291 Relative expression of *SP1* compared to GAPDH from *SMYD5*-KO cells, measured by RT-qPCR at 37°C,
292 with or without rescue with Flag-SMYD5 sgRNAres plasmid (labelled SMYD5 sgRNA#6res). *SMYD5*-KO
293 leads to increased expression of *SP1* showing that effect is secondary to targeting of *SMYD5* but not
294 something else. Data shown as in (E). (G) Western blot quantification and representative figure using
295 antibodies against SMYD5 and Lamin B in a *SMYD5*-KO cell line with and without rescue with Flag-
296 SMYD5 sgRNAres plasmid (labelled SMYD5 sgRNA#6res) shows that *SMYD5*-KO was successful on
297 protein level at 37°C. Data shown as in (E). (H-J) Western blot quantification and representative
298 figure using antibodies against SP1, CIRBP and RBM3, respectively, in *SMYD5*-KO cells. Shown are
299 data points, each data point is a biological replicate, mean and SD where applicable. Significance
300 levels were calculated with unpaired one-tailed t-test in GraphPad Prism. * = P<0.05, ** = P<0.01,
301 *** = P<0.001, **** = P<0.0001.

302

303 SMYD5 shows temperature dependent expression *in vitro* and *in vivo.*

304 To test whether SMYD5 shows differential expression levels at 37°C and 32°C, we performed
305 immunofluorescence staining using a custom antibody against SMYD5[51]. We observe nuclear and
306 cytoplasmic staining of SMYD5 at 37°C (SMYD5; white or green, DAPI; purple, **Figure 5A, top**). The
307 expression of SMYD5 was significantly decreased at 32°C compared to 37°C (**Figure 5A and S11A**).
308 We observed a statistically significant (P<0.05) difference of SMYD5 intensity comparing the two
309 temperatures at the whole cell level (**Figure 5B**). Upon limiting to nuclear SMYD5-levels at the two
310 temperatures we see a trend towards less SMYD5 in the nucleus at 32°C when compared to 37°C
311 (**Figure 5C**). We also validated using an anti-FLAG antibody in cells with overexpression of SMYD5-
312 FLAG[44], which yielded a similar result (**Figure S11B**). We validated further by performing a Western
313 blot from HEK293 at 32°C and 37°C, showing significantly less SMYD5 at 32°C when compared to 37°C
314 (**Figure 5D**). This difference was not noted at the transcriptional level (**Figure 5E**) indicating that
315 SMYD5, is primarily regulated post-transcriptionally. Finally, we show that the brains of mice cooled
316 in a standard regimen used to treat neonatal asphyxia[52] show a similar temperature-dependent
317 decrease in SMYD5 after 6 h of cooling (**Figure 5F**), indicating that SMYD5-dependent impact on the
318 MHR during a standard TTM regimen in mice.

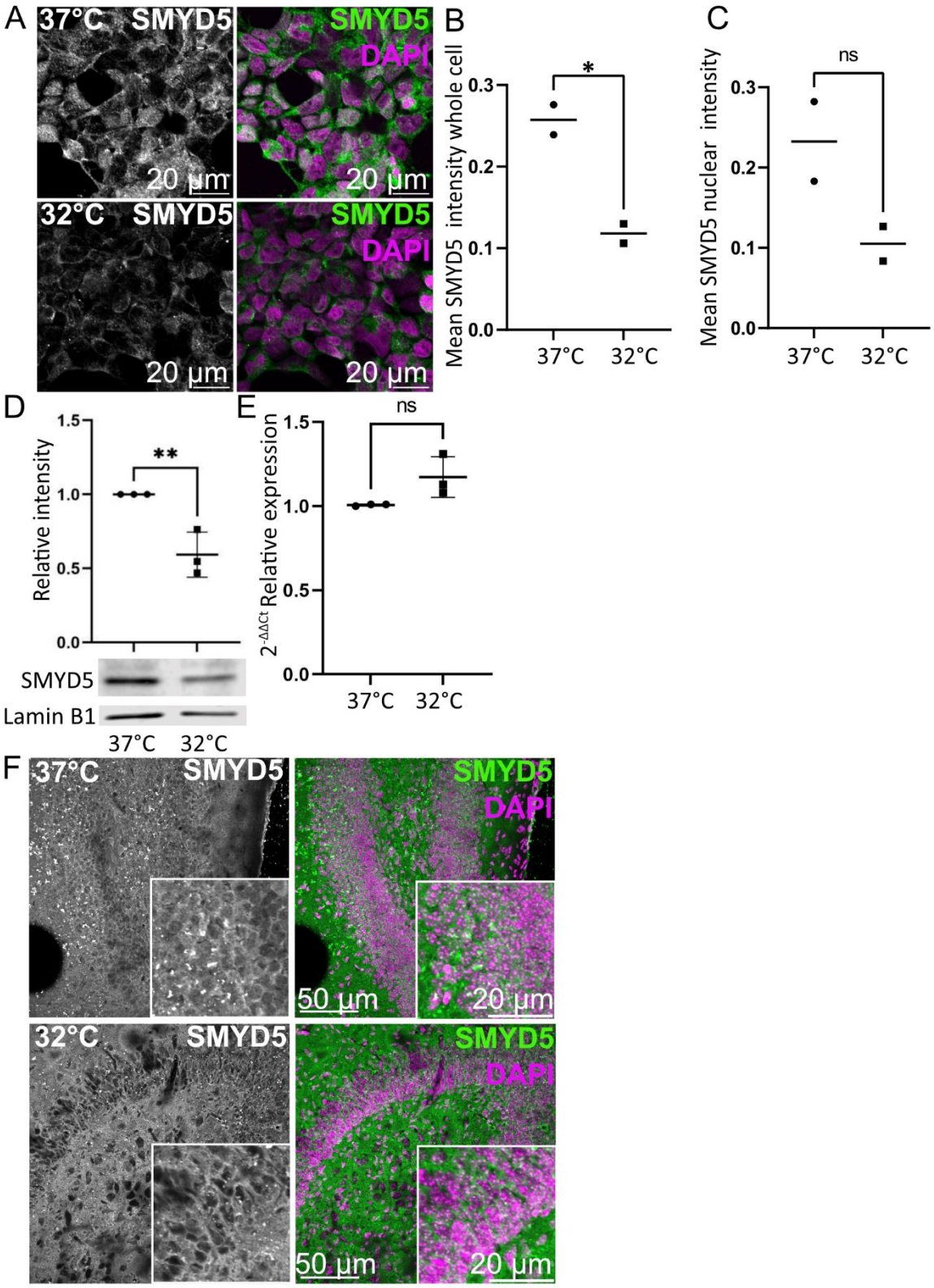

Figure 5. SMYD5 is degraded at 32°C *in vitro* and *in vivo*. (A) Intensity of endogenous SMYD5 at 37°C (left) and 32°C (right), 6 h incubation. (B) Quantification of cellular SMYD5 intensity. Shown are data points, each data point is a biological replicate, mean where applicable. Significance levels were calculated with unpaired two-tailed t-test in GraphPad Prism. (C) Quantification of nuclear SMYD5 intensity. Data shown as in (B). (D) Western blot and quantification using SMYD5 antibodies at 37°C

325 and 32°C, 6 h incubation. Significance levels calculated with one-tailed t-test in GraphPad Prism
326 otherwise data shown as in (B). (E) qRT-PCR results for SMYD5 expression at 37°C and 32°C, 6 h
327 incubation. Data shown as in (D). (G) Less SMYD5 staining in mice that had been cooled down to 32°C
328 compared to mice kept at euthermia 37°C in brain slices from the hippocampal region of a mouse
329 model of TTM. * = P<0.05, ** = P<0.01, *** = P<0.001, **** = P<0.0001.

330 Epigenetic and transcriptional consequences of temperature-dependent changes in
331 SMYD5.

332 As SMYD5 is decreased at 32°C and SMYD5-binding peaks overlap a CpG-island (**Figure 4A**),
333 we also performed DNA methylation (DNAm) analysis using the 850 K EPIC Illumina array and
334 observed limited DNAm at 16/18 sites and no differential DNAm at *SP1*, *CIRBP* or *RBM3* promoters at
335 32°C for 6 h compared to 37°C at CpG´s spanning the gene regions (**Figure S12, Supplementary Table**
336 **6**). However, there was differential DNAm at other CpGs loci after 6 h exposure at 32°C
337 (**Supplementary Table 7**) supporting the idea that the MHR may be regulated by the epigenetic
338 machinery. To further explore the epigenetic consequences of differential SMYD5 availability at 37°C
339 versus 32°C, we performed CUT&RUN using antibodies against H3K36me3, H4K20me3, H3K9me3,
340 H3K4me3, H3K27me3, SMYD5 and H3 (control) in HEK293 cells and human neural progenitor cells
341 (NPCs). We choose H3K36me3, H4K20me3 and H3K9me3 since these modifications have been
342 previously shown to be deposited by SMYD5[44,45]. We also chose to look at H3K4me3 and H3K27me3
343 as these are general open and closed chromatin modifications and are also known to change during
344 vernalization in plants[53]. We saw less H3K36me3 over *SP1* at 32°C compared to 37°C in NPCs (**Figure**
345 **6A**) and HEK293 cells (**Figure S13A**) as well as decreased global SMYD5 binding (**Figure 6B**), all
346 consistent with lower SMYD5 amounts at 32°C (**Figure 5**). We further observed a global deficiency of
347 H3K36me3 at 32°C compared to 37°C seen in both HEK293 cells and NPCs but more prominent in
348 NPCs (**Figure 6C, Figure S13B**) indicating that this modification is used to regulate additional genes
349 perhaps through SMYD5 but levels of SMYD5 mirror this effect (**Figure 6B**, **Figure 5B-5E**). We also
350 observed a global H3K4me3 deficiency at 32°C compared to 37°C (**Figure 6D**), although there were
351 also 1288 genes that had a unique H3K4me3 modification at 32°C which was not seen at 37°C
352 (**Supplementary Table 8**). For H3K9me3 we saw a deficiency of histone modification marks upstream
353 of gene bodies in NPCs (**Figure 6E**). We did not see a difference for other histone modification when
354 comparing 32°C and 37°C in NPCs (**Figure S13C-S13D**). CUT&RUN for H3K36me3 also revealed a
355 number of significantly differentially modified genes at 32°C when compared to 37°C (**Figure 6F,**
356 **Figure S13E, Figure S14, Supplementary Table 5**) including a number of epigenetic regulators such as
357 *SETD1B* and *BAZ2A* (**Figure 6F, Figure S14A, Figure S14E**). To identify additional genes regulated by
358 SMYD5 and temperature, we performed RNASeq in mouse NPCs (mNPCs) at the two temperatures.
359 This yielded 2890 differentially expressed genes (DEGS) that were upregulated and 3133 that were

360 downregulated at 32°C compared to 37°C. Interestingly, when we overlap upregulated DEGS in
361 mNPCs at 32°C with SMYD5-bound and repressed genes (*Smyd5*-KO upregulated) at 37°C in mESCs
362 we observe a statistically significant overlap of 26 genes (P=5.4e-04, **Figure 6G**). Similarly, when we
363 overlap down-regulated DEGS in mNPCs at 32°C with SMYD5-bound and upregulated genes (*Smyd5*-
364 KO downregulated) at 37°C in mESC we also observe an overlap of 19 genes (P=0.029, **Figure 6H**).
365 This suggests that SMYD5 regulates additional genes in a similar manner to *SP1* (as a repressor at
366 euthermia) as well as regulating some in an inverse manner (normally as an activator at euthermia)
367 in murine models. This includes several genes upregulated at 32°C with a theoretically appealing role
368 for hypothermia responses such as *Klf15* (role in brown adipose tissue metabolism)[54] and *Thrap3*
369 (role in thyroid metabolism and adipocyte differentiation)[55,56]. Among the genes normally
370 upregulated at 37°C but down-regulated at 32°C, *Bnip3L*, a pro-apoptotic gene[57] is of particular
371 interest given the previously observed cytoprotective role of mild hypotherma[10–12]. We provide the
372 entire list of 45 SMYD5-temperature dependent genes as **Table 1.** When we looked more closely at
373 the list of genes that had unique H3K4me3 modification in NPCs at 32°C and overlapped those genes
374 with human orthologs of upregulated DEGS in mNPCs at 32°C we saw a significant overlap of 169
375 genes (P=2.4e-03, **Figure 6J, Supplementary table 9**). Only 6 genes are bound by SMYD5 and
376 upregulated with *Smyd5*-KO at 37°C in mESCs as well as upregulated at 32°C in mNPCs (**Table 1**) and
377 have a unique H3K4me3 peak at 32°C in NPCs (**Supplementary table 8**). Interestingly *Asxl1,* a
378 member of the Polycomb family[58] a family which is known to take part in vernalization in plants[48], is
379 among these 6 genes. This indicates that there may be additional epigenetic MHR-responses that are
380 independent of SMYD5. Finally, we demonstrate that on average these 45 genes, regulated by
381 SMYD5, have lower H3K36me3 modifications at 32°C versus 37°C at their gene bodies as well as
382 fewer modifications over the 3'-UTR region at 32°C in NPCs and HEK293 cells (**Figure S13F-S13G**). As
383 well as, these genes show a different H3K4me3 and H3K9me3 modification pattern at 32°C and 37°C
384 when looking at their 3'- and 5'-UTR regions (**Figure S13H-S13J**).

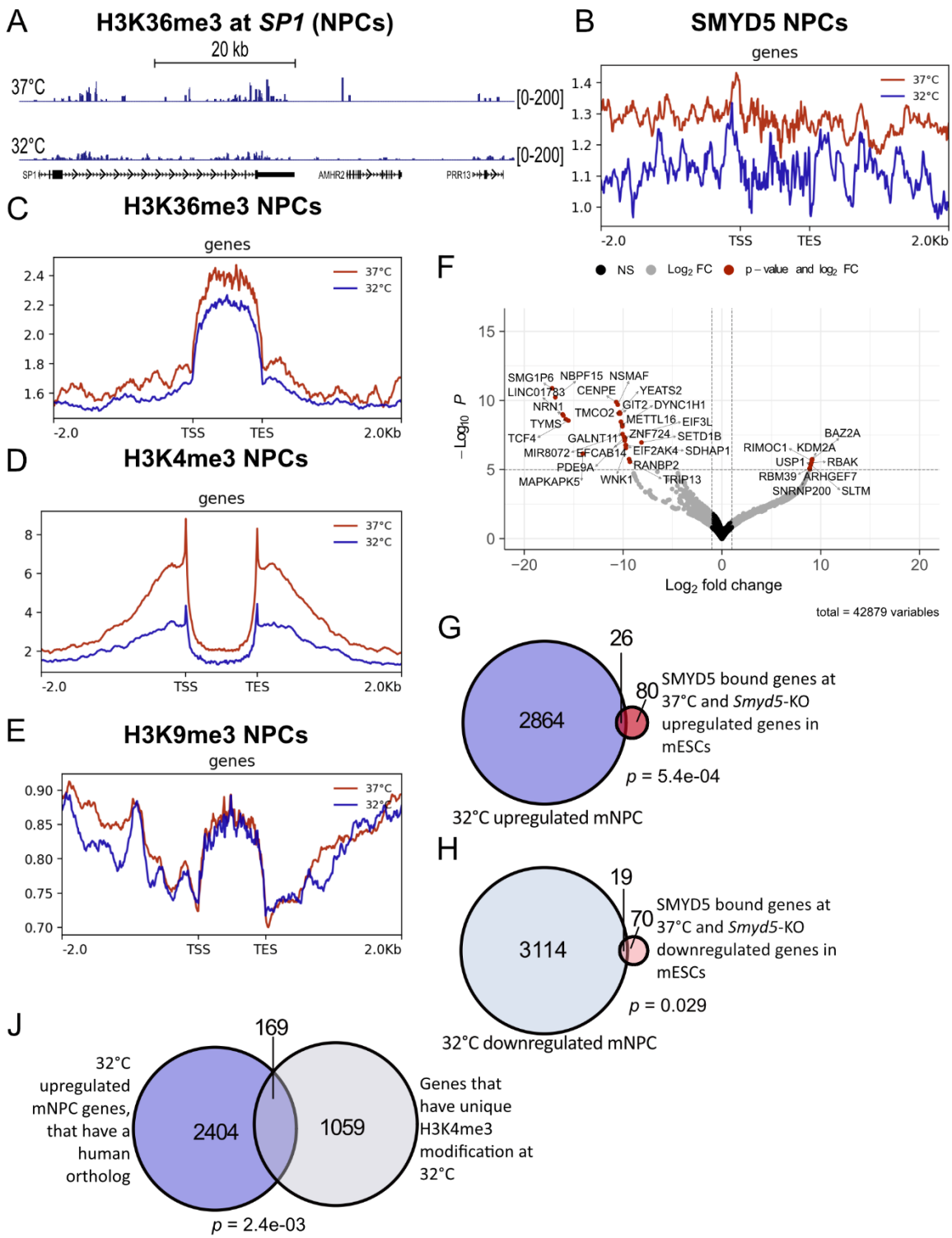

Figure 6. SMYD5 is a novel epigenetic gatekeeper of the MHR. (A) Increased H3K36me3 is observed at the *SP1* promoter and genebody at 37°C compared to 32°C. (B) SMYD5 chromatin binding is globally decreased (all genes) at 32°C compared to 37°C. (C) There is a global deficiency of H3K36me3 at 32°C compared to 37°C. (D) There is a global H3K4me3 deficiency at 32°C compared to 37°C. (E) Upstream of gene bodies there is a global H3K9me3 deficiency at 32°C compared to 37°C. (F) At the gene-specific levels there are a number of genes, that have more or less H3K36me3 at 32°C compared to 37°C in NPCs. Red circles indicated genes that have Log_2 fold change over 1 and p-value

393 less than 10^{-6}, gray circles indicate Log_2 fold change over 1 but non-significant p-value and black
394 circles indicate non-significant genes. (G-H) DEGS from RNASeq in mNPCs at both temperatures,
395 show overlap with SMYD5-bound genes that are differentially expressed upon *Smyd5*-KO in mESCs at
396 37°C. Statistical analysis done with GeneOverlap package in R using Fisher's Exact test. (J) There is an
397 significant overlap of DEGS and genes that have a unique H3K4me3 modification at 32°C. Statistical
398 analysis as in (G-H).

SMYD5-repressed genes ↑ at 32°C (SMYD5 represses at 37°C)

Gene	Function	Role
Mybl2	Transcription factor	Cell-cycle control
Klf15	Transcription factor	Brown-tissue metabolism
Thrap3	Transcriptional co-activator	Thyroid hormone receptor binding
Tex15	DNA repair protein	Role in testicular meiosis
Ewsr1	RNA binding	Role in Ewing sarcoma
Tfcp2l1	Transcription factor	Pluripotency in stem cells
Amotl2	Angiostatin binding factor	Role in angiogenesis
Phf20	Methyllysine-binding protein	Histone modification
Cd24a	Sialoglycoprotein	Cell differentiation
Nt5e	Nucleotidase	Nucleotides metabolism
Neo1	Cell surface receptor	Immunoglobulin superfamily
Gabbr1	GABA receptor	Inhibitory neurotransmitter
Asxl1	Chromatin binding protein	Polycomb family member
Tulp4	Tubby Superfamily Protein	Ubiquitination function
Pkn1	Serine/threonine-protein kinase	Protein kinase C superfamily
Hnrnpul1	RNA-binding protein	hnRNP family
Mier1	Transcriptional regulator	Mesoderm induction early response
Fam21	WASH complex member	Endosomal protein sorting
Trip12	E3 ubiquitin-protein ligase	Ubiquitin regulation and DNA repair
Lamc1	Extracellular matrix glycoprotein	A laminin
Rell1	RELT-like protein	Regulates the p38MAPK cascade
Xrn2	5'-3' exonuclease	Promotes transcription termination
Hspg2	Multidomain proteoglycan	Encodes Perlecan protein
Ctc1	Telomere maintenance protein	Limits telomere degradation
Stag1	Component of cohesin complex	Role in cohesion of sister chromatids
Ass1	Enzyme	Role in urea cycle

SMYD5-upregulated genes ↓ at 32°C (SMYD5 activates at 37°C)

Gene	Function	Role
Usp28	Ubiquitin Thioesterase	DNA damage checkpoint
Ccnd1	Cyclin D	Cell cycle regulation
Dzip3	Ubiquitin-protein transferase	Spermatogenesis
Rad50	DNA double-strand break repair	Cell cycle regulation
Arglu1	Enables cadherin binding	Mediator complex
Sltm	RNA binding activity	Regulation of transcription
Slc16a3	Solute transporter	Lactic acid and pyruvate transport
Ier5l	Unknown function	Parolog of IER5
Acly	Enzyme	Synthesis of cytosolic acetyl-CoA
Agps	Enzyme	Lipid biosynthesis

Apobec3	Cytidine deaminase	RNA editing
Ivns1abp	Viral binding protein	Response to viral infection
Dus3l	Synthesis of dihydrouridine	RNA editing
Upp1	Uridine phosphorylase	Ribonucleosides dynamics
Ldha	Enzyme	Lactate to Pyruvate conversion
Scd2	Enzyme	Fatty acid biosynthesis
Smarcad1	Chromatin remodeler	Role in heterochromatin formation
Bnip3l	Pro-apoptotic protein	Induces apoptosis
Esrra	Nuclear receptor	Mitochondrial biogenesis regulator

Table 1: Summary of temperature responsive SMYD5-regulated genes.

Discussion

Histone modification has previously been found to help integrate the effects of cold temperature exposure in diverse organisms. For example, in plants, vernalization is the basis of how cold exposure influences the rate of flowering is mediated through a Trithorax-Polycomb switch[48]. In some reptiles, sex determination is achieved through a temperature dependent mechanism and for one such, the red eared slider turtle (*Trachemys Scripta Elegans*), the mechanistic basis of this regulation acts through a histone methylation switch[47]. To uncover additional regulators of the MHR we used the MHI to identify an FDA-approved drug, Entacapone, that can induce the SP1-mild hypothermia response as well as conducting a forward CRISPR-Cas9 mutagenesis screen resulting in recognition of *SMYD5* as a repressor of the MHR at euthermia. Such agents can be useful to understand the mechanistic underpinnings of the MHR but also for therapeutic development for patients at risk of neurological sequela after catastrophic events.

Our current MHIs allow for some temporal dissection yet they all currently harbor stable fluorescent protein, which may be less time sensitive to detecting dynamic differences compared to real time qPCR. Thus, our current MHIs may be the most useful to map the start of the response (as we have done in **Figure 1**). However, in future work, we hope to create unstable fluorescent molecules that break down quickly to help us map the kinetics of different parts of the response, for example how quickly the response is resolved (i.e. termination).

Although, our drug screen and validation may have limitations (only three timepoints, single dose), we observe an overrepresentation of TKIs. The reason why some TKIs as well as other drugs did not validate could be as the drug screen was performed using an MHI containing the MCRE (to increase signal) but validation was performed on a MHI lacking the MCRE (endogenous situation in mammals[15]). Of the TKIs we have further shown that Poziotinib, a known pan-HER inhibitor[29], was able to increase *RBM3* mRNA but not *SP1* or *CIRBP* mRNA (**Figure S7**) or SP1 (**Figure 2F**) at 37°C with

424 the single dose tested. The lack of increased SP1 quantified by Western blot could be caused by low
425 (4 µM) Poziotinib dosage compared to RT-qPCR and flow cytometry (20 µM). Here, we did identify
426 and validated Entacapone as a compound that can activate the SP1-MHR at euthermia (**Figure 2E**).
427 Interestingly, Entacapone is COMT-inhibitor which increases dopamine availability with blocking its
428 degradation in synapses[59] and it is known that synaptic plasticity can be influenced with temperature
429 changes.[60] Furthermore, Entacapone is a neurotransmitter breakdown inhibitor (COMT), supporting
430 the fact that several candidates (**Figure 3C-3D**) from the CRISPR-Cas9 forward mutagenesis screen
431 appear to bind the neural synapse and/or Syntaxin (**Supplementary table 3**) such as *STXBP1* (SP1
432 repressor) and *TXLNB* (SP1 activator) which bind to Syntaxin (**www.genecards.org**), and play a role at
433 the neuronal synapse as well as having a role in dopaminergic synaptic transmission[61]. which may be
434 worth exploring in future work.

435 Our data support the notion that SP1 and RBM3 may be parts of individual arms of the
436 mammalian hypothermia response as SMYD5 only regulates *SP1* but not *RBM3*. We interpret the lag
437 in the response (at least 6 hours to signal) and the obvious shift in fluorescence of mutagenized cells
438 to mean that there are likely many genes upstream of the currently tested point of the response
439 (*SP1*). Despite a global shift towards activators, the yield from the enrichment screen yielded more
440 putative *SP1* repressors compared to *SP1* activators. This could be caused by the setup of the screen
441 as it may be easier to find genes that increase fluorescence (repressors) than those with decreased
442 fluorescence (inhibitors) which may overlap with cells that have lost the SP1-MHI for various reasons.
443 Another limitation to our forward screen is it can only identify cell-autonomous genes and cannot
444 find essential genes. However, it is a starting point, and it has already provided several candidates
445 that can be subsequently tested for effect using our MHIs. Of interest, SMYD5 and ERBB2/HER2 (the
446 receptor Poziotinib blocks) have been previously found to functionally interact in a forward
447 mutagenesis screen of genes that play a role in metastatic reactivation and tumor dormancy[62] and
448 additionally *CIRBP* transcript levels, correlates with prognosis in for luminal A/B breast cancer which
449 is influenced by HER2 status[63]. In fact, our SP1-repressor screen revealed several downstream factors
450 of ERBB2 signaling (*RAS*, *ERK*, *STAT5,* **Figure S7A**), indicating that this pathway may be upstream of
451 SMYD5 and worth exploring. Alternatively, SP1 itself may be a target of phosphorylation, and as SP1
452 is predicted to bind at its own promoter[64], perhaps both signals are required for full effect.

453 Here, by uncovering *SMYD5* as a negative epigenetic regulator of SP1, a key factor of the
454 mammalian MHR, we provide an example of how histone methylation integrates temperature cues
455 into a fundamental pathway in mammals. Our present model is that SMYD5 exerts its effects at 37°C
456 to ensure that *SP1*/*CIRBP* are not upregulated without the cold stimulus, however, upon cold
457 stimulus (32°C), SMYD5 is degraded or its protein synthesis is degraded enough to lead to loss of

458 SMYD5 levels and thus allows the pathway to proceed. Global cellular SMYD5 levels are decreased at
459 32°C *in vivo* and *in vitro* (**Figure 5**) as well as there is a trend towards less SMYD5 in the nucleus at
460 32°C (**Figure 5C and 5F**) this could happen as a result of nuclear exclusion of SMYD5 or there could be
461 less *SMYD5* translation or SMYD5 could undergo proteasomal degradation. Per bioGRID, SMYD5 is
462 bound to four ubiquitinators (PARK2, UBA52, TRIM25, USP34) so this may be an avenue for further
463 study as such factors often target proteins to the proteasome. Previously, decreased production of
464 protein upon cold stimulus has shown to act through AMPK mediated phosphorylation of eEF2K[22],
465 and decreased translational efficiency could play a part. But we are unaware of biological examples
466 of directed protein degradation in response to mild hypothermia. This requires further investigation.

467 SMYD5 itself appears to regulate at least 45 other factors that show temperature
468 dependence, 26 in which SMYD5 acts as a repressor (like *SP1*) and another 19 where SMYD5 acts as
469 an activator at euthermia. Some of these genes look very plausible MHR participants, especially
470 *BNIP3L,*[57] a pro-apoptotic factor which is down-regulated with hypothermia and may thus contribute
471 to the neuroprotective effect of mild hypothermia. There are also genes that play a role in thyroid
472 and adipocyte function (*THRAP3*)[55,56], brown adipose tissue (*KLF15*)[54] and testes (*TEX15*)[65,66], all
473 target tissues for mammalian temperature responses. Coinciding with decreased global H3K4me3 at
474 32°C, we also observed decreased H3K36me3 at 32°C over the gene *SETD1B* which encodes a
475 H3K4me3-methyltransferase (**Figure 6 and S14E**). In oocytes *Setd1b*-KO can cause gain or loss of
476 H3K4me3[67]. Accordingly, this could be one potential mechanism underlying H3K4me3 changes at
477 32°C and warrants further investigation. It is interesting that H3K36me3 has previously been shown
478 to regulate temperature-regulated alternative splicing in plants[68] and in the fungus *Saccharomyces*
479 *cerevisiae,* H3K4 and H3K36 methyltransferases (Set1 and Set2) regulate alternative
480 polyadenylation[69] as well as in mice H3K36me3 has a direct impact on alternative splicing of
481 rewarding neurobiological factors in the brain[70]. In mammals temperature dependent alternative
482 splicing[71] and alternative splicing of *CIRBP* and *RBM3* has been observed[72–74]. Perhaps alternative
483 splicing or polyadenylation plays a role for *SP1* or one of the other 45 SMYD5-bound factors
484 elucidated here.

485 In summary, we have developed and validated tools to interrogate the MHR, and used them
486 to show for the first time that a compound exists that can activate the MHR as well as shone light on
487 potential regulatory genes in the MHR pathway. We show that *SMYD5* is a temperature-dependent
488 epigenetic gatekeeper of the MHR and for the first time we show how histone methylation signature
489 (H3K36me3, H3K9me3 and H3K4me3) change in mammals with MHR exposure, providing a specific
490 example of how mammalian cells use epigenetics to respond to temperature cues.

Acknowledgements: We thank SCRU lab (UI) for gifting us pMD2.G (Addgene, #12259) and psPAX2 (Addgene, #12260) and H.C. Dietz and D. Valle labs (JHU), for gifting us the HCT-116, SK-N-SH, HeLa, Jurkat and K562 cell lines. We want to thank Alan Long at the ChemCore facility at JHU and Pharmacy of Landspitali for support regarding the drug screen and validation. We thank the Immunology department of Landspitali University Hospital for the access and assistance with the FACS sorting. We thank Funlab at deCODE genetics for the usage of their flow cytometry machines as well as for gifting us the HEK293T cell line. We thank Kári Stefánsson and Ólafur Þ. Magnússon at deCODE Genetics for providing some of the next generation sequencing for this project. We thank Erna Magnúsdóttir for providing pAG-MNase for the CUT&RUN assays as well as guidance with the CUT&RUN experiment and data analysis. This study was supported with funding from the Rannis Technology Development Fund (H.T.B., #2010588), Eimskip University Fund (S.R.), Fulbright Iceland (S.R.), Icelandic Cancer Society Research Fund (H.T.B.), Göngum Saman Research Fund (H.T.B.), Landspitali Research Fund (H.T.B.), Félag Háskólakvenna Research Fund (S.R.). HTB is also supported by funding from Rannís (#217988, #195835, #206806) and the Louma G. Foundation. Finally, some images in this manuscript were created with BioRender.com.

Author contributions: H.T.B. and S.R. conceptualized project. S.R., L.Z. and H.T.B. created and designed the MHIs. S.R., A.T., L.H.A., M.V., K.E.A. and K.J. performed cell culture. S.R., A.T. L.H.A. and M.V. performed flow cytometry experiments. L.Z. and H.T.B. designed the approach to the drug screen. S.R. and H.T.B. designed the approach to the forward mutagenesis assay. S.R. performed the forward mutagenesis assay and drug screen. S.R. and K.J.A. performed the PCR for the NGS. S.R., A.T. and K.J. validated results from drug and mutagenesis screens (Western blots (A.T., K.J.), RT-qPCR (S.R., K.J.) and flow cytometry (S.R., A.T.)). K.J and K.M. performed IF on cells from culture and K.J. and K.M performed the confocal imaging and K.M., K.J. S.Th.H. and S.R. did the analysis. S.R. and M.V. performed siRNA knockdown. R.C-V. and F.J.N. provided mouse brains treated with TTM. K.J.A. isolated and cultured mNPCs. M.V. performed cryosectioning and IF on mouse brain slices and M.V. and K.M. performed confocal imaging as well as the analysis of the mouse brain slices. S.R., A.T. and S.Th.H. performed CUT&RUN experiments. K.J.A. did the mNPCs isolation and RNASeq and data analysis. S.R., K.J.A., K.J., A.T. S.Th.H. and T.R. analyzed data. J.H. provided SMYD5 antibody and K.E.A. provided human NPCs. S.R. and H.T.B. wrote the manuscript. Project administration was carried out by H.T.B, S.R and K.J.A.

Declaration of interest: Dr. Bjornsson is a consultant for Mahzi therapeutics. Dr. Rafnsdottir and Dr. Bjornsson have a European patent application pending with the number 23167505.9.

524 **STAR Methods**

525 **Creation of novel indicators:** We used the PGL4.10 plasmid (Promega, #9PIE665) as the backbone for
526 our CIRBP- and SP1-MHI, where the *luc2* sequence was cut from the plasmid with NcoI (NEB,) and
527 XbaI (NEB). Promoter sequence for *CIRBP*[75] was cloned from mouse sequence using *CIRBP* forward
528 primer 5'tcgataggtaccTGGCTTCACAAATGCGCCTCAGT3' and *CIRBP* reverse primer
529 3'cctaaggcagatctGCGAGGGGGAGCGCAAGAGT5'[75]. Restriction enzymes KpnI (NEB) and BglII (NEB)
530 were used to insert the promoter into the plasmid. Promoter sequence for *SP1*[76] was cloned from
531 human DNA using the forward primer 5'tcaagtcaggctagcGCAACTTAGTCTCACACGCCTTGG3' and
532 reverse primer 3'cagtgctgcctcgagGCTCAAGGGGGTCCTGTCCGG5'[76]. Restriction enzymes NheI (NEB)
533 and XhoI (NEB) were used to insert the promoter into the plasmid. AcGFP1 was cloned from
534 PT7XbG2-AcGFP1 (Novopro, #V002843) vector using the reverse primer
535 3'cggcggagTCTAGAATTACTTGTACAGCTCGTCC5' and the forward primer
536 5'taagccaccATGGTGAGCAAGGGCGAGGAGC3'. Restriction enzymes NheI (NEB) and XhoI (NEB) were
537 used to insert the acGFP1 into the plasmid. The neomycin selection cassette was cloned from
538 pROSA26-dest plasmid (Addgene, #21189) using the forward primer
539 5'CATTATCGTCGACTCTACCGGGTAGGGGAGGCGCTT3' and reverse primer
540 3'CGCCGCCGACGATAGTCAAGCTTCTGATGGAATTAGAACTTGGC5'. Restriction enzymes SalI (NEB) and
541 PshAI (NEB) were used to insert the neomycin cassette into the plasmid. CIRBP- and SP1-MHI were
542 made with and without MCRE[15]. The MCRE sequence was inserted in 5 repeats in front of the
543 promoter sequences with a linker sequence between. Acc65I (NEB) restriction enzyme was used to
544 insert the MCRE sequence into the CIRBP-MHI and Acc65I (NEB) and SacI (NEB) restriction enzymes
545 were used to insert the MCRE into the SP1-MHI. Sanger Sequencing was used to validate insertion
546 sites, size, and sequence of insertion. The *RBM3* promoter with MCRE enhancer (6 repeats) in front
547 of the promoter was cloned into the multiple cloning site pCMV6-AC-GFP (BlueHeron, #PS100010).
548 We also made lentiviral vectors for *CIRP*, *SP1* and *RBM3* on a pLV-Ex (VectorBuilder) lentiviral vector.
549 The *CIRBP* promoter for the CIRBP-lenti-MHI was designed from the human promoter and the *SP1*
550 promoter was moved upstream of the TSS for the SP1-lenti-MHI but *RBM3* promoter sequence
551 remained unchanged. Included were MCRE (8 repeats for CIRBP-lenti-MHI, 5 repeats for other),
552 promoter, neomycin selection cassette and mCherry fluorescent protein behind each promoter
553 sequence. The promoter region, size and backbone plasmid for each indicator is detailed in
554 **Supplementary Table 1** and sequence of each MHI in **Supplementary File 1**. We also observed some
555 variation in absolute levels among individual indicators/experiments, but the pattern was always
556 consistent; given this, we only show data from individual experiments in any figure.

557 **Culture of cell lines:** HEK293 (gifted and DSMZ, CRL-1573, referred to as 293/293WT) cells were
558 cultured in DMEM/F12 with GlutaMAX (Gibco, 10565018) with 10% filtered FBS (Gibco, 10270106)
559 under 5% CO_2. Cells were cultured at 37°C unless otherwise stated, then 37°C served as a control. In
560 addition to HEK293, we used the following cell types HEK293T (gifted, CRL-3216), HCT-116 (gifted,
561 CCL-247), HeLa (gifted, CCL-2), Jurkat (gifted, TIB-152), K562 (gifted, CCL-243), SK-N-SH (gifted, HTB-
562 11), human iPS cells (ATCC, 1019) that were used to generate NPCs by neural induction of iPSCs using
563 dual SMAD inhibition and embryoid body generation (StemCell Technologies; 08581, 05832,
564 05838)[77], prior to experiments described here the NPCs were cultured in STEMdiff Neural Progenitor
565 Medium (StemCell Technologies, 05833) on Matrigel (Corning). As well as murine primary NPCs (see
566 section mNPC isolation for further information). We used culture recommendations from ATCC when
567 possible. Cells were sub-cultured when they had reached 70-90% confluence and media was changed

568 every other day. Killing curves were used for all cell lines to determine lowest selection concentration
569 for all selection agents.

570 **Transfection of MHI and SMYD5-Flag overexpression plasmid:** HCT116, 293WT, HEK293T, HeLa and
571 SK-N-SH cell lines were transfected with MHI when they had reached 70-90% confluency. We used
572 either Lipofectamine™ 2000 or 3000 (Thermo Fisher Scientific, 11668027, L3000015) according to
573 the manufacturer's protocol. The fluorescence of the indicators was measured via flow cytometry up
574 to 48 h after transfection. We analyzed flow cytometry data with the FlowJo Software, where we
575 gated on living cells, single cells, GFP positive cells and measured the fluorescence for that
576 population. For further analysis, we used Excel from Microsoft, GraphPad Prism (v.9) and FlowJo
577 (v.10.8.1). All statistical testing was done with GraphPad Prism (v.9). For transfection of SMYD5-Flag
578 overexpression vector[44] we used the same method as described above.

579 **Construction of 293WT+Cas9 and 293WT+Cas9+SP1 cell lines:** We made two cell lines from 293
580 cells, one that expressed Cas9 (lentiCas9-blast, Addgene #52962), referred to as 293WT+Cas9, and
581 another that expressed both Cas9 and our SP1-MHI, referred to as 293WT+Cas9+SP1. These cell lines
582 were made by transfecting the plasmids with lipofectamine as described above and selecting stably
583 transfected cells using Blasticidin selection for Cas9 and Neomycin selection for our SP1-MHI.

584 **Drug screen:** Briefly, we used Lipofectamine 3000 (Thermo Fisher Scientific, L3000015) to transfect
585 the SP1+MCRE-MHI into the 293T cell line. 24 h after transfection, 30000 cells were plated into each
586 well of a black 96 well plate. 48 h after transfection the cells were exposed to FDA Approved Drug
587 Screening Library (L1300-Z298012) via the High Throughput Screening Services, ChemCore Facilities
588 (Johns Hopkins University). Each drug was exposed in 20 µM final concentration. Total well GFP was
589 read with the CLARIOStar Plus Plate Reader (BMG LABTECH, settings: gain 1500, 470-15 excitation
590 and emission 515-20 at focal height 2.6) 16, 28, and 40 h after exposure of the library. Ratio of
591 increased fluorescence was calculated by dividing GFP reads from positive control (SP1+MCRE-MHI
592 transfected but untreated) at each time point with GFP reads of each whole well exposed to drug at
593 the same timepoint for wells in the same lane. For further analysis, we used Excel from Microsoft and
594 GraphPad Prism (v.9).

595 **Validation of drug screen:** We individually validated 8 compounds in same concentration (20 µM).
596 Here, we exposed the drug for 16 h, and evaluated by flow cytometry as previously described. In a
597 96-well plate 20,000 of either 293 or 293+SP1-MHI cells were seeded per well in a total volume of
598 200 µL of media. After cells had attached to the wells (the morning after), cells were exposed to 20
599 µM of each drug, controls were exposed to the same quantity of DMSO as drug, for 16 h and
600 harvested for flow cytometry analysis. Flow cytometry analysis was conducted as previously
601 described. Drugs that were tested for further validation after initial screen were: Orantinib
602 (Selleckchem, S1470), Dasatinib (Selleckchem, S7782), Poziotinib (Selleckchem, S7358), Tamoxifen
603 Mylan (Mylan AB*), Erythromycin (Stragen Pharma GmbH*), Naloxone (B. Braun*), Entacapone
604 (Orion Corporation*) and Cinacalcet (Ratiopharm GmbH*). Drugs labeled with "*" were
605 pharmaceutical grade medications gifted from the Pharmacy at Landspítali University Hospital.
606 Analysis was performed as described above.

607 **Apoptosis assay:** We based our apoptosis assay on that published by Xiang et al[78]. We exposed
608 293WT+Cas9+SP1 cell line either to 1-5 µM H_2O_2 or vehicle (H_2O) for 4 h at 32˚C or 37˚C. 4 h after
609 exposure gMFI of the cells were analyzed with flow cytometry as described above.

610 **Genome Wide CRISPR-Cas9 screen on fluorescent HEK293WT cell lines that stably express SP1-**
611 **MHI:** Using the 293WT+Cas9+SP1 and 293WT+Cas9 (negative control) cell lines we performed a
612 GeCKO screen, where we transduced the sgRNA pool made from library A and B (Addgene,
613 #1000000049) in MOI 0.3[17–19]. We mostly followed the Joung et. al. protocol[19], the exceptions are as
614 follows. For making the lentivirus, a protocol described by Kutner et. al[79] was used. Lentiviral sgRNA
615 library concentration was done with Amicon ultracentrifugal filters (Millipore, UFC9003). 20 h after
616 transduction with the sgRNA library selection was started with puromycin and continued for 6 days
617 and 8 h before the cells were moved to 32˚C, where they were incubated 16 h before fluorescent
618 activating cell sorting (FACS) sorting with Cell sorter SH800Z (Sony). The 5% highest fluorescent cells
619 for 293WT+Cas9+SP1 and and 5% lowest fluorescent cells for 293WT+Cas9+SP1 were sorted. Next,
620 we isolated gDNA and performed a two step PCR for all samples (sorted as well as negative control).
621 According to cell number after puromycin selection, the sgRNA library coverage was >700 times
622 coverage for HEK293WT+Cas9+SP1. Next generation sequencing (NGS) with single read with 80
623 cycles and 8 indexing cycles with PhiX spike in of 20% on NovaSeq S4 at deCODE genetics for
624 HEK293WT+Cas9+SP1 and HEK293WT+Cas9, 32-280 million aligned reads per sample. To analyze the
625 screen data, single read fastq files for each replicate and condition were merged using cat command.
626 Then, MAGeCK (v.0.5.9) was used to identify enriched sgRNA's in sorted samples[33,80] and sgRNA
627 counts were normalized to internal control for sgRNA's (control sgRNAs). We used RStudio (R,
628 v.4.1.1)[81] to visualize the results and to filter genes. We exported a list of genes that had both FDR
629 value under 0.25 and LFC value over 2.5 for each condition in both screens. Then, we excluded genes,
630 overrepresented in both the repressor and activators screen when compared to control as they most
631 likely promote cell growth and therefore were present in both lists. For the pathway enrichment
632 analysis we used EnrichAnalyzer() from MAGeCKFlute (v.1.12.0)[80].

633 **Making of *SMYD5* knockout (*SMYD5*-KO) cells:** Two ready-made sgRNA vectors (Genscript, *SMYD5*
634 plasmid vector #2 and #6) were packed into lentivirus according to protocol described by Kutner et.
635 al[79], for concentration we used the 4x Lentivirus concentrator solution protocol from the MD
636 Anderson Cancer center at University of Texas (available online). We selected for stable *SMYD5*-KO
637 cells with puromycin selection for at least 7 days.

638 **Making of *MALT1* and *RGS21* knockout cells**: Ready made sgRNA vectors (Genscript, plasmid vector
639 *MALT1* #1 and #2, *RGS21* plasmid vector #2 and #3) were packed into lentivirus and selected as
640 described above in the making of *SMYD5-KO* cells.

641 **Making of gRNA resistant SMYD5-Flag plasmid (**Flag-SMYD5 sgRNAres plasmid)**:** In an effort to make
642 SMYD5-Flag resistant to CRISPR-Cas9 cutting from our two guides (guide 2&6), we used site-directed
643 mutagenesis (Q5® Site-Directed Mutagenesis Kit, New England Biolabs) to modify predicted PAM
644 sites of the guides (Genscript, SC1678, plasmid vector #2 and #6). We used the following primers to
645 induce the mutations: SMYD5-2mut-F: 5'-gctctttacgAGGAAGCAGTCAGCCAGT-'3; SMYD5-2-mut-R: 5'-
646 ttccgtaaagAGTCTCCGCAGAAGTTCC-'3; SMYD5-6-mut-F: 5'-accgatatcgAGCCTGTGACCACTGCCT-'3;
647 SMYD5-6-mut-R: 5'-atagagcgtt-CCAGAGAAACTGTGCAGCC-'3. After site-directed mutagenesis, we
648 isolated plasmid with Monarch Midiprep kit (New England Biolabs) and Sanger sequenced to verify
649 changes in PAM-sites. This plasmid was then used for rescue experiments (**Figure 4E-4F**).

650 **siRNA:** We used the TriFECTa RNAi kit (IDT; TYE 563 Transfection Control DsiRNA, 51-01-20-19
651 (transfection control); Negative Control DsiRNA, 51-01-14-03 (negative control)) and used

652 predesigned DsiRNA (IDT, hs.Ri.SMYD5.13.8) to knockdown *SMYD5* mRNA in two biological clonal cell
653 lines of HEK293+Cas9+SP1-MHI with Lipofectamine 2000 (Thermo Fisher Scientific, 11668027) with
654 reverse transfection, where we seeded $1*10^6$ cells per well in a 6 well plate. One batch of cells was
655 exposed to 32°C and the other to 37°C for 6 hours. Data were analyzed with flow cytometry 36 h
656 after transfection. Further statistical analysis of the flow cytometry data was similar to that described
657 above.

658 **Immunofluorescence of cell culture:** HEK293 cells were seeded into an 8-well chamber slide and
659 then fixed and permeabilized with 4% PFA and 0.1% Triton-X 100 diluted in PBS for 10 mins at room
660 temperature. Then cells were washed twice with a blocking solution comprising PBS with 2.5% BSA
661 and 10% normal goat serum and followed by blocking for 30 mins in the blocking solution. Cells were
662 incubated overnight with primary antibodies (rabbit anti-SMYD5, 1:1000[51]; anti-FLAG, 1:500, (Sigma-
663 Aldrich, F1804-200UG)) at 4°C. The following day, cells were incubated at room temperature for 30
664 mins and then washed three times every 10 mins with a washing solution composed of PBS with
665 0.25% BSA. Cells were incubated with secondary antibodies (goat anti-mouse IgG (H+L) Alexa Fluor™
666 488, 1:1000 (Invitrogen™, A-11001); goat anti-rabbit IgG (H+L) Alexa Fluor™ 647, 1:1000
667 (Invitrogen™, A21244)) for 1 h at room temperature in the dark. Cells were washed three times every
668 10 mins with the washing solution and added with Fluoromount-G Mounting Medium with DAPI
669 (Invitrogen, 00-4959-52). Cells were imaged using confocal microscopy (FV 1200, Olympus
670 Fluoroview) using a 30x silicon objective (NA1.05). Images were processed by ImageJ[82,83] and
671 quantified using CellProfiler (v.4.2.5.)[84] . Statistics were calculated in GraphPad Prism.

672 **Real Time Quantitative Polymerase Chain Reaction (RT-qPCR):** Total RNA from cells incubated at
673 32°C or 37°C was isolated, using Direct-zol™ RNA Microprep (Zymo Research, R2062), according to
674 the manufacturer's instructions. The concentration of RNA was measured by NanoDrop (Thermo
675 Fisher Scientific) followed by cDNA synthesis with High-Capacity cDNA Reverse Transcription Kit
676 (Applied Biosystems, 4368814) on MiniAmp™ Thermal Cycler (Applied Biosystems™). RT-qPCR was
677 performed using Luna® Universal qPCR Master Mix (NEB, M3003) on CFX384™ Real-Time PCR
678 Detection System (Bio-Rad). Each biological replicate of the RT-qPCR assay in this study was carried
679 out in technical triplicates. Any technical replicate that deviated from other replicates by ≥ 0.4 cycle
680 threshold (Ct) was removed from calculations of average Ct values. The primers used are as follows:
681 SP1 (fwd): 5'-CACCCAATTCAAGGCCTGCCGT-3'; SP1 (rev): 5'-GGGTTGGGCATCTGGGCTGTTT-3'; RBM3
682 (fwd): 5'-GAGACTCAGCGGTCCAGGGGTT-3'; RBM3 (rev): 5'-CCTCTGGTTCCCCGAGCAGACT-3'; CIRBP
683 (fwd): 5'-CCGAGTTGACCAGGCTGGCAAG-3'; CIRBP (rev): 5'-TCCATAGCCCCGGTCTCCTCCT-3'; GAPDH
684 (fwd): 5'-TCAAGGCTGAGAACGGGAAG-3'; GAPDH (rev): 5'-CGCCCCACTTGATTTTGGAG-3'. SMYD5 1
685 (fwd): 5'-GCACTGTGCGCAAAGACCTCCA-3', SMYD5 2 (fwd): 5'-GGAAACCAGGCCAGGTTCTGCC-3',
686 SMYD5 3 (fwd) 5'-CGTGGAAGTCCGTTTCGTGA-3', SMYD5 1 (rev:) 5'-CTGGGCACAGGACCTGGTGGTA-
687 3', SMYD5 2 (rev): 5'-GGCTGCCAACCGACATTCTGCA-3', SMYD5 3 (rev) 5'-CCAGAGAAACTGTGCAGCCA-
688 3'.

689 **Western blot assay:** Cells were washed with PBS and then lysed for 30 min on ice in RIPA buffer
690 (50mM Tris HCl ph8, 150mM NaCl, 1% NP-40, 1% Sodium deoxycholate, 0.1% SDS, 2mM EDTA,
691 phosphatase inhibitor (either Cell signaling, 5870S or Thermo Fisher Scientific, 78437)). The lysate
692 was centrifuged at 16,000 xg for 20 min at 4°C and the supernatant was collected. The supernatant
693 was diluted with 4X loading buffer (LI-COR, 928-40004) and heated at 95°C for 5 min. The protein
694 concentration was measured using Pierce™ BCA Assay Kit (Thermo Fisher Scientific, 23225). 20-30 µg

695 of protein was loaded into each well and separated by SDS-PAGE. They were transferred to
696 polyvinylidene fluoride (PVDF) membranes and blocked in 5% bovine serum albumin in Tris-buffered
697 saline with Tween 20 for 1 hour. Primary antibodies: rabbit anti-CIRBP, 1:2000 (Proteintech, 10209-2-
698 AP); rabbit anti-RBM3, 1:1000 (Proteintech, 14363-1-AP); rabbit anti-SP1 1:1000 (Proteintech, 21962-
699 1-AP); mouse anti-Lamin B1, 1:5000 (Proteintech 66095-1-Ig); rabbit anti-SMYD5, 1:1000[51]; mouse
700 anti-GAPDH, 1:5000 (Abcam, ab8245) were applied to respective membranes after washing, and
701 incubated at 4˚C overnight. Membranes were incubated with IRDye® secondary antibodies; anti-
702 rabbit (LI-COR,926-32213); anti-mouse (LI-COR, 926-68072), at room temperature for 90 mins. After
703 washing, the protein bands were visualized on the Odyssey® CLx Infrared Imaging System and protein
704 band intensity quantified by Image J software.

705 **DNAm studies and analysis:** 293WT (biological triplicates) were split into two batches and exposed
706 to 37°C and 32°C for 6 h, next cells were harvested and DNA isolated with the Zymo Quick-DNA™
707 Midiprep Plus Kit (Zymo Research, D4075). Samples were submitted to the Genetic Resources Core
708 Facility (Johns Hopkins University), bisulfite treated, and run on the Infinium MethylationEPIC
709 BeadChip Kit (Illumina) with two technical controls (50% and 100% DNAm, 8 samples total). Technical
710 controls were created using mixtures of 100% and 0% methylated HCT116 DKO (Zymo, Research
711 D50414-1/2). DNA methylation data (IDAT files) containing unmethylated and methylated intensity
712 values were imported to R (v.4.2.1) for analysis[81]. Raw data was processed using single sample
713 approach with preprocessNoob() function and methylation values (beta values) were obtained using
714 the getBeta() function from minfi package (v.1.42.0)[85–87]. The model matrix was created for the two
715 temperatures using the model.matrix() function from stats R package and sva() function from sva
716 package (v.3.44.0) was applied with two estimated surrogate variables[81,88]. The model was fit with
717 contrast matrix using lmFit(), with the estimated coefficients and standard errors generated using
718 contrasts.fit() from limma package (v.3.52.4)[85,89]. The p-values were moderated using eBayes()
719 function from limma package (v.3.52.4) and CpG cites ranked according to their p-value[89].

720 **CUT&RUN:** 293WT and human NPCs (ATCC, cat. ACS-1019) were harvested and CUT&RUN performed
721 according to Epicypher CUTANA protocol (v.1.7) on 300.000 cells per sample. We permeabilized the
722 cells with 0.01% digitonin (Sigma, D141). For normalization we spiked in E. Coli DNA (Epicypher,
723 23618-1401) at the final concentration of 0.2 ng per sample. The library preparation was performed
724 with TrueSeq-Chip Sample preparation Kit (Illumina, IP-202-9001). The following antibodies were
725 used for the CUT&RUN: CTCF antibody (Cell Signaling, 2899S), H3K36me3 (Thermo Fisher Scientific,
726 MA5-24687), H4K20me3 (EpiCypher, 13-0054), H3K9me3 (Abcam, ab176916), H3K4me3 (EpiCypher,
727 13-0041), H3K27me3 (Thermo Fisher Scientific, MA5-11198), SMYD5 [51], and Rabbit IgG Antibody
728 (Epicypher, 23613-0042). For the CUT&RUN analysis and the CUT&TAG re-analysis we followed
729 published STAR protocols[90]. Briefly, first we trimmed the raw Fastq reads in paired mode with
730 TrimGalore (v.0.6.7)[91] then we used Bowtie2 (v.2.4.4.)[92] to align the reads to Hg38 or mm10 and E.
731 Coli reference genome, all downloaded from UCSC. Overall alignment to Hg38 were from 83.6-
732 98.63% and to E. Coli spike in were from 0.1-4.18% for our data. The aligned Sam files were then
733 converted to Bam files, indexed, and sorted via SAMtools (v.1.15)[93] and BedGraphtoBigWig (v.4)[94]
734 from BEDTools (v.2.3)[95]. We used SEACR (v.1.3)[96] for peak calling after normalization with the
735 normalization factor calculated as 1/(percent alignment to E. coli). We used DiffBind (v.3.9.6)[97] for
736 the differential peak analysis, ChIPseeker (v.1.35.3)[98], TxDb.Hsapiens.UCSC.hg38.knownGene
737 (v.3.4.6)[99] and org.Hs.eg.db (v.3.8.2)[100] for annotation. For further analysis and image creation we
738 used deepTools (v.3.5.1.)[101] and R [81].

739 **Mouse NPC isolation:** Mouse NPCs were isolated from the cortex of E17.5 C57BL6/NTac embryos.
740 The protocol was adapted from Bernas et al, 2017[102]. Embryo cortices were manually dissected from
741 brains and the tissue was dissociated in 1X TrypLE™ Select Enzyme (Thermo Fisher Scientific,
742 A1217701) for 10 min, with manual dissociation using a 1000 µL pipette. The cell suspension was
743 washed in Neurobasal medium (Thermo Fisher Scientific, 21103049) and filtered through a 70 µm
744 cell strainer (Miltenyi Biotech, 130-110-916). Cells were washed 2X in 5 mL Neurobasal medium
745 (Gibco, 21103049) by centrifugation at 200 xg for 10 min. Cells were resuspended in 1 mL Neurobasal
746 growth medium containing 1X B27 supplement (Thermo Fisher Scientific, 17504044), 1X
747 Penicillin/Streptomycin (Thermo Fisher Scientific, 15140122), 1X Glutamax (Thermo Fisher Scientific,
748 35050038), 20ng/mL FGF-2 (Peprotech, 100-18B), 20 ng/mL EFG (Peprotech, AF-100-15), and 2
749 µg/mL Heparin (MP Biomedicals, 210193125). Cells were seeded onto 12-well plates, previously
750 coated for 2 h at 37°C in 1:100 dilution of Matrigel (Corning, 354234). After passaging, NPCs were
751 cultured in media described above on plates coated overnight in poly-D-lysine (Sigma, P7280), and
752 then coated for 2 h in laminin (Sigma, L2020). Cells were either sub-cultured or media was changed
753 every 2 days.

754 **RNAseq:** Primary mouse NPC lines from 4 separate embryos were seeded 0.3 x 10^6 cells per well, in
755 two batches, in a poly-D-lysine/laminin coated 6-well plate after 9 days *in vitro*. Following 36 h of
756 incubation at 37°C, one plate with 4 lines was incubated at 32°C for 6 h. Cells from both 37°C and
757 32°C conditions were harvested in tri-reagent and RNA was isolated using the Direct-zol RNA
758 Microprep kit (Zymo Research, R2063). RNAseq library construction and Illumina next generation
759 sequencing was performed by Novogene, generating 30 million paired-end reads per sample. For the
760 RNAseq analysis, Fastq files were pseudo-aligned to the GRCm39 mouse transcriptome, downloaded
761 from NCBI, using Kallisto (v.0.48.0) with paired-end mode on and 100 bootstraps. Kallisto output files
762 were imported into R using the tximport package[103]. Transcripts were assigned to genes using the
763 TxDb.Mmusculus.UCSC.mm10.ensGene package (v.3.4.0) [104] in R . Differential expression analysis was
764 performed using the DESeq2 package (v.3.16)[105] in R after discarding transcripts with less than 10
765 counts. Differentially expressed genes were defined as those with an adjusted p-value less than 0.1.
766 Overlaps of gene lists were calculated using the GeneOverlap package (v.1.34.0)[106] in R, with overlaps
767 tested using Fisher's exact test. Gene set enrichment analysis was performed using the GSEA-
768 preranked program[107,108] with the Mouse Ortholog Hallmark Gene Sets[109]. For the GSEA-pre-ranked
769 run, we generated a ranked gene list comprising all detected genes assigned to a rank value, which
770 was calculated as -log10(adjusted p-value) × (sign of fold change). The genes were then ranked from
771 the highest rank value to the lowest before inputting into the program.

772 **Mouse cooling followed by immunostaining on brain slices:** C57BL6 mice (Jackson) were bred to
773 create a litter (n=2). At P10, we split littermates into two groups. One group (n=6) was cooled to a
774 core temperature of 32°C and the other (n=6) maintained at 37°C, for 6 hours respectively. These
775 animals were then euthanized, and their brains were isolated immediately after the cooling period
776 and flashed with PBS. One of the hemispheres was immersed in 4% PFA for 72-96 h for fixation and
777 the other hemisphere was dissected for the cerebellum, thalamus/basal ganglia, hippocampus,
778 anterior and posterior cortex. After fixation, samples were cryopreserved in a sucrose gradient and
779 then flash-frozen. Frozen hemispheres were cryosectioned with the help of a cryostat (Keldur, UI).
780 The sections were washed in TBS+ (TBS (LiCor, 927-60001) with 0.05% triton X-100(Sigma-Aldrich,
781 T8787-100ML)) twice for 10 minutes. Next, the slides were immersed in DAKO (target retrieval
782 solution, sodium citrate buffer, pH 6) at 95°C for 20 minutes. Slides were then washed again in TBS+

783 twice for 10 minutes. Next, the slides were blocked in TBS++ (TBS (LiCor, 927-60001) with 3% goat
784 serum (Abcam, ab7481)) for 1 h at room temperature. The slides were then stained with primary
785 antibodies and anti-rabbit-SMYD5, 1:200, for 24 h at room temperature and carried out in the dark.
786 On the next day, slides were allowed to reach room temperature before they are washed 3x for 10
787 minutes in TBS+. The slides were incubated with secondary antibodies, goat anti-mouse IgG (H+L)
788 Alexa Fluor™ 488, 1:1000 (Invitrogen™, A-11001); goat anti-rabbit IgG (H+L) Alexa Fluor™ 647, 1:1000
789 (Invitrogen™, A21244), for 24 h in the dark and washed 3x for 10 minutes in TBS+. All the liquid on
790 the slides was briefly dried off. Fluoromount-G Mounting Medium with DAPI (Invitrogen, 00-4959-52)
791 was placed on each section and covered with a cover slip. The slides were incubated for 24 h at room
792 temperature before being imaged using confocal microscopy (FV 1200, Olympus Fluoroview) using a
793 30x silicon objective (NA1.05). Images were processed by ImageJ[82,83] and quantified using CellProfiler
794 (v.4.2.5.)[84] . Statistics were calculated in GraphPad Prism.

795

796 **Supplementary Tables and Files**

797 **List of Supplementary Tables**

798 **Supplementary Table 1**: Specifics of MHIs (word file).

799 **Supplementary Table 2**: Top 91 drug hits from MHI screen (excel file).

800 **Supplementary Table 3**: Top candidate genes found enriched in mutation screening (excel file).

801 **Supplementary Table 4:** Genes found in both repressor and activator SP1 lists and thus excluded for
802 further evaluation (excel file).

803 **Supplementary Table 5:** Top differentially modified locations for H3K36me3 in NPCs from CUT&RUN
804 experiment (excel file).

805 **Supplementary Table 6**: List of CpGs represented at three genes (word document).

806 **Supplementary Table 7**: List of differentially methylated locations from EPIC DNAm array (excel file).
807 **Supplementary Table 8:** List of genes that have a unique H3K4me3 histone modification peak at 32°C
808 (excel file).

809 **Supplementary Table 9**: List of genes that show DEGS at 32°C and have a unique H3K4me3 histone
810 modification peak at 32°C (excel file).

811

812 **Supplementary files**

813 **Supplementary File 1:** Sequences of individual MHIs.

814 **Supplementary figures**

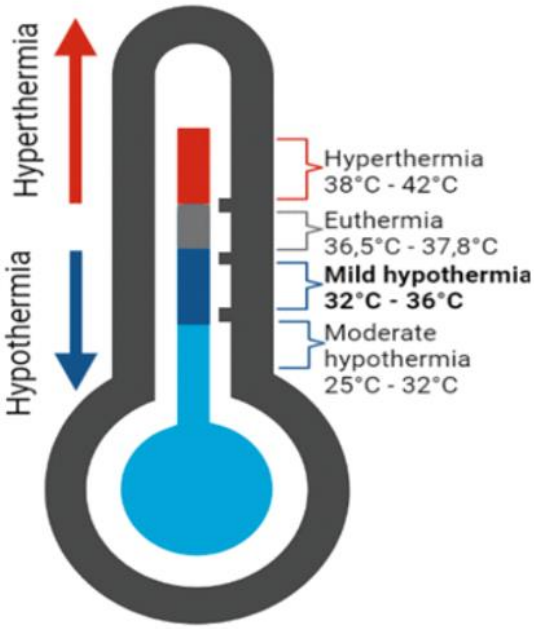

815

816 **Figure S1. Different temperature ranges.** Temperatures known to induce distinct responses
817 (moderate and mild hypothermia, euthermia and hyperthermia). Our range of interest (mild
818 hypothermia) is bolded.

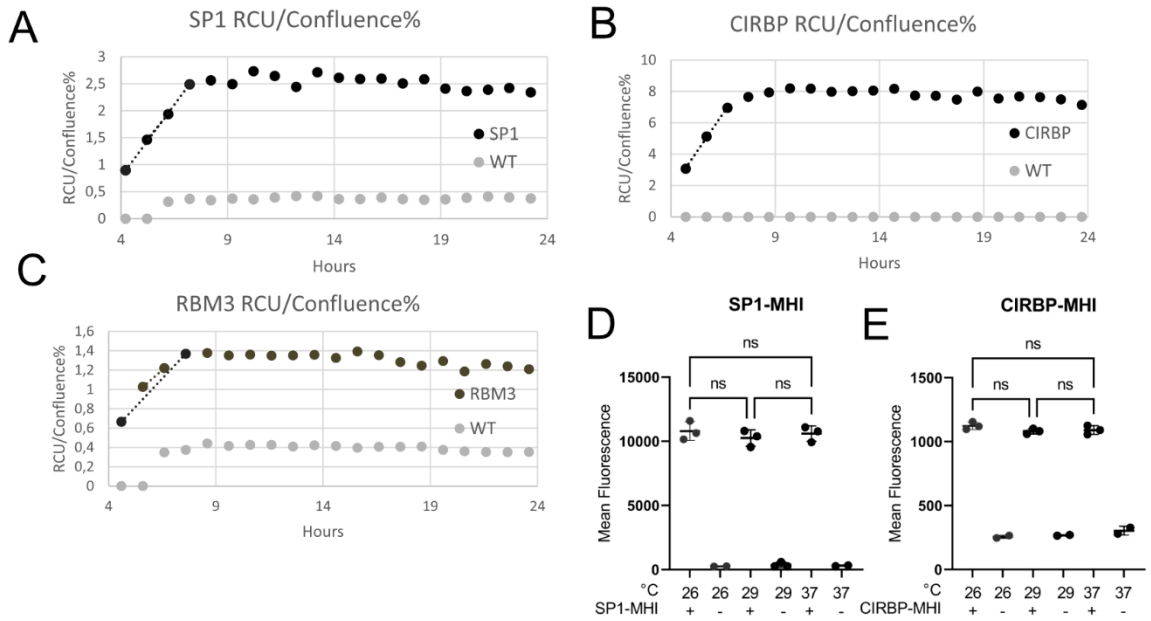

Figure S2. MHI activation peaks during mild hypothermia (32˚C) and is limited at other temperatures. (A-C) We measured fluorescence hourly using an IncucyteS3 at 32˚C using SP1-Lenti-MHI, CIRBP-Lenti-MHI, RBM3-Lenti-MHI respectively. (D-E) No increased fluorescence was observed at moderate hypothermia for either SP1-MHI or CIRBP-MHI in HEK293 cells. * = P<0.05, ** = P<0.01, *** = P<0.001, **** = P<0.0001.

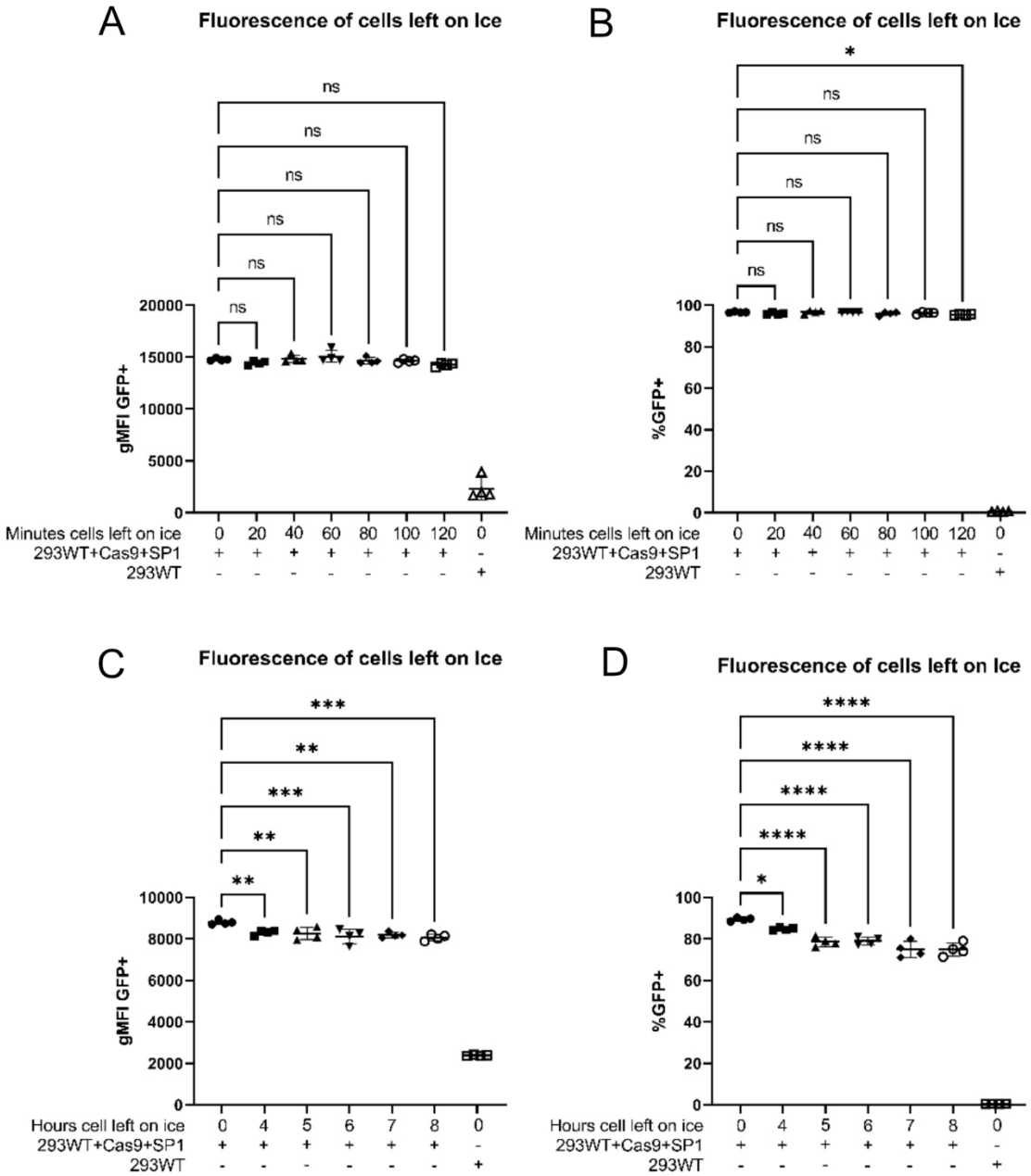

Figure S3. Storage of samples on ice does not lead to activation of MHI. (A-B) gMFI or percentage of fluorescent cells of HEK293WT+Cas9+SP1 (293WT cell line expressing SP1-MHI) left on ice for different periods of time before flow cytometry analysis. Shown are data points, each data point is a technical replicate, mean and SD where applicable. Dunnett's multiple comparison test calculated in GraphPad Prism. (C-D) Mean fluorescence or percentage of fluorescent cells of HEK293WT+Cas9+SP1 left on ice for different periods of time before flow cytometry analysis. Data shown as in (A), independent replicate. * = P<0.05, ** = P<0.01, *** = P<0.001, **** = P<0.0001.

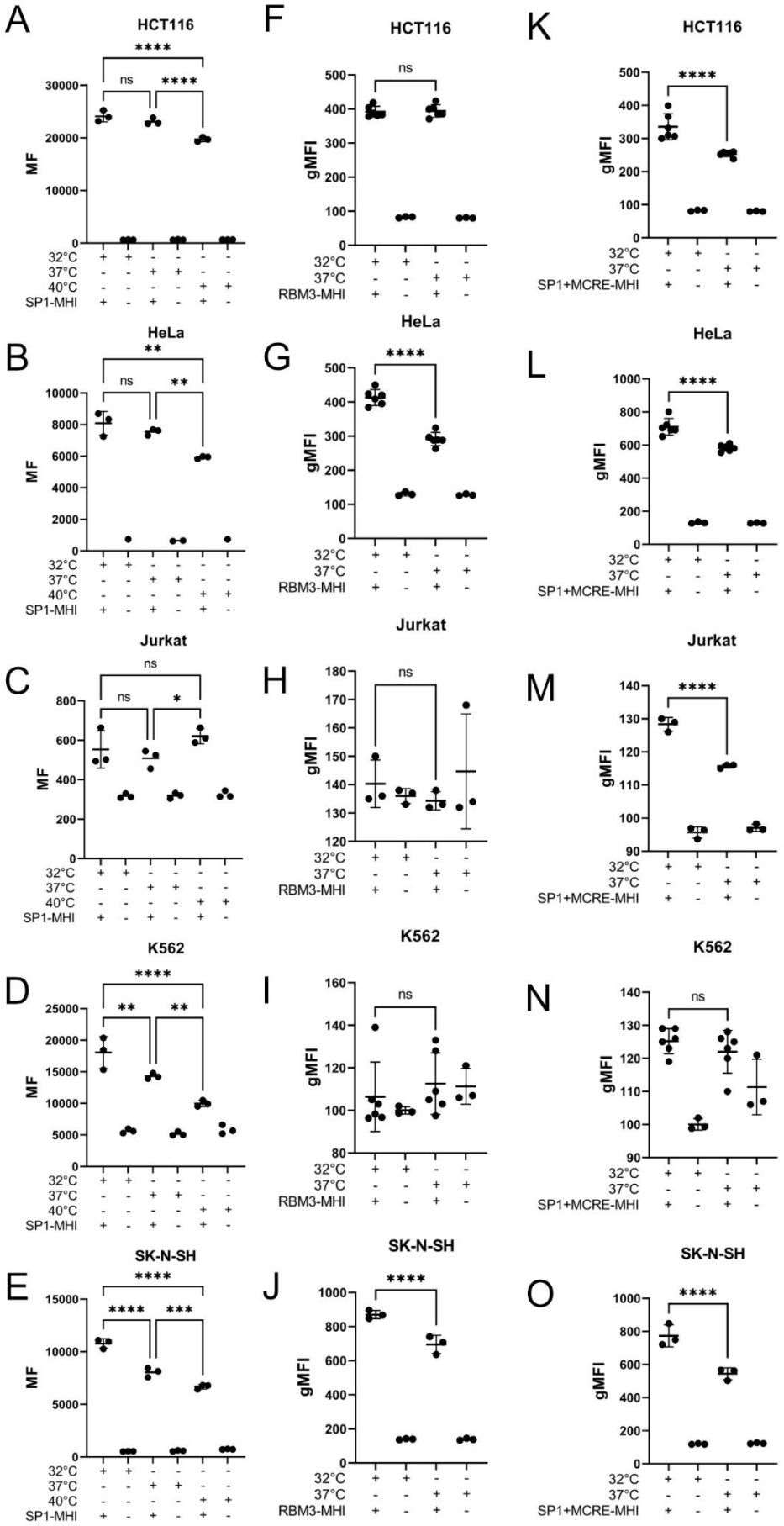
A
HCT116
MF
32°C
37°C
40°C
SP1-MHI
B
HeLa
C
Jurkat
D
K562
E
SK-N-SH
F
HCT116
gMFI
RBM3-MHI
G
HeLa
H
Jurkat
I
K562
J
SK-N-SH
K
HCT116
SP1+MCRE-MHI
L
HeLa
M
Jurkat
N
K562
O
SK-N-SH

835

836 **Figure S4. MHI demonstrate consistent activation at 32°C in diverse cellular systems.** (A-E) Left
837 column shows mean fluorescence (MF, flow cytometry) after transient transfection of SP1-MHI
838 into HCT116, HeLa, Jurkat, K562 and SK-N-SH (16 h at 32°C, 37°C and 40°C). Shown are data
839 points, each data point is a technical replicate, mean and SD where applicable, Šidák's multiple
840 comparison test calculated in GraphPad Prism. (F-J) Middle column shows gMFI (flow cytometry)
841 after transient transfection of RBM3-MHI into HCT116, HeLa, Jurkat, K562 and SK-N-SH (16 h at
842 32°C and 37°C). Data shown as in (A-E). (K-O) Right column shows gMFI (flow cytometry) after
843 transient transfection of SP1+MCRE-MHI into HCT116, HeLa, Jurkat, K562 and SK-N-SH (last 16 h
844 at 32°C and 37°C). Data as in (A-E). * = P<0.05, ** = P<0.01, *** = P<0.001, **** = P<0.0001.

845

846

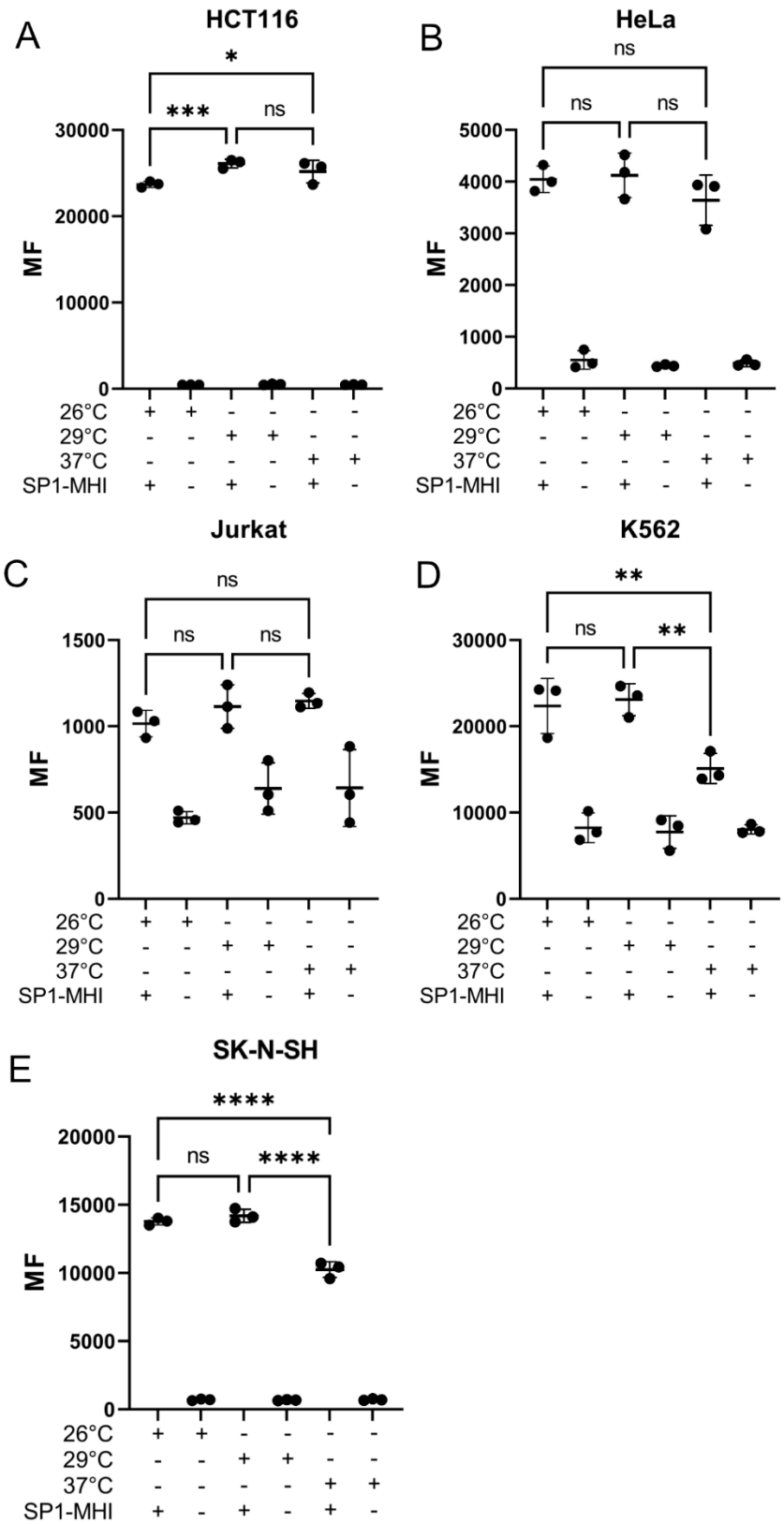
A
HCT116
*
***
ns
MF
30000
20000
10000
0
26°C + + - - - -
29°C - - + + - -
37°C - - - - + +
SP1-MHI + - + - + -
B
HeLa
ns
ns
ns
MF
5000
4000
3000
2000
1000
0
26°C + + - - - -
29°C - - + + - -
37°C - - - - + +
SP1-MHI + - + - + -
C
Jurkat
ns
ns
ns
MF
1500
1000
500
0
26°C + + - - - -
29°C - - + + - -
37°C - - - - + +
SP1-MHI + - + - + -
D
K562
**
ns
**
MF
30000
20000
10000
0
26°C + + - - - -
29°C - - + + - -
37°C - - - - + +
SP1-MHI + - + - + -
E
SK-N-SH
****
ns
****
MF
20000
15000
10000
5000
0
26°C + + - - - -
29°C - - + + - -
37°C - - - - + +
SP1-MHI + - + - + -

847

848 **Figure S5. Moderate hyperthermia does not activate SP1 MHI in diverse systems.** (A-E) Mean
849 fluorescence of SP1-MHI as measured by flow cytometry after transient transfection of MHI into
850 HCT116, HeLa, Jurkat, K562, SK-N-SH (16 h at 26°C, 29°C and 37°C). Shown are data points, each
851 data point is a technical replicate, mean and SD where applicable. Šidák's multiple comparison. *
852 = P<0.05, ** = P<0.01, *** = P<0.001, **** = P<0.0001.

853
854

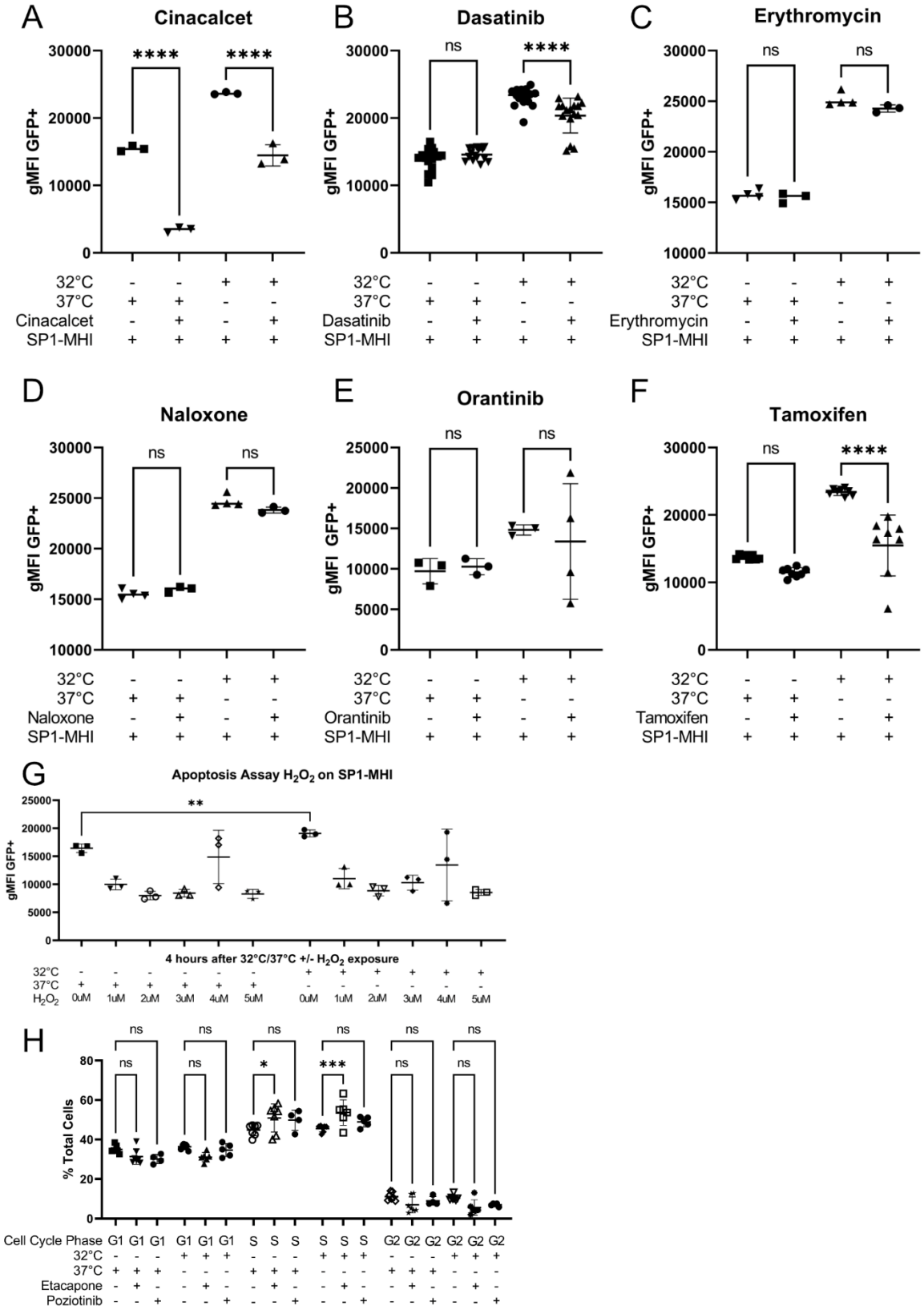

Figure S6: Individual validation of potential hits from drug screen. (A-F) gMFI measured with flow cytometry of HEK293WT cell line that stably expresses MHI after 16 h of Cinacalcet (A), Dasatinib (B), Erythromycin (C), Naloxone (D), Orantinib (E), and Tamoxifen (F) at 32°C or 37°C.

Shown are data points, mean and SD where applicable. Šidák's multiple comparison calculated with GraphPad Prism. (G) Cell cycle analysis done with PI staining. Mean fluorescence measured for G1, S and G2 phases of the cell cycle with flow cytometry of HEK293WT cell line 16 h after Entacapone or Poziotinib exposure at 32°C or 37°C. Data shown as in (A-F). (H) Apoptosis analysis done with H_2O_2 exposure. Shown are data points, mean and SD where applicable. Unpaired t test calculated with Graphpad Prism. * = P<0.05, ** = P<0.01, *** = P<0.001, **** = P<0.0001.

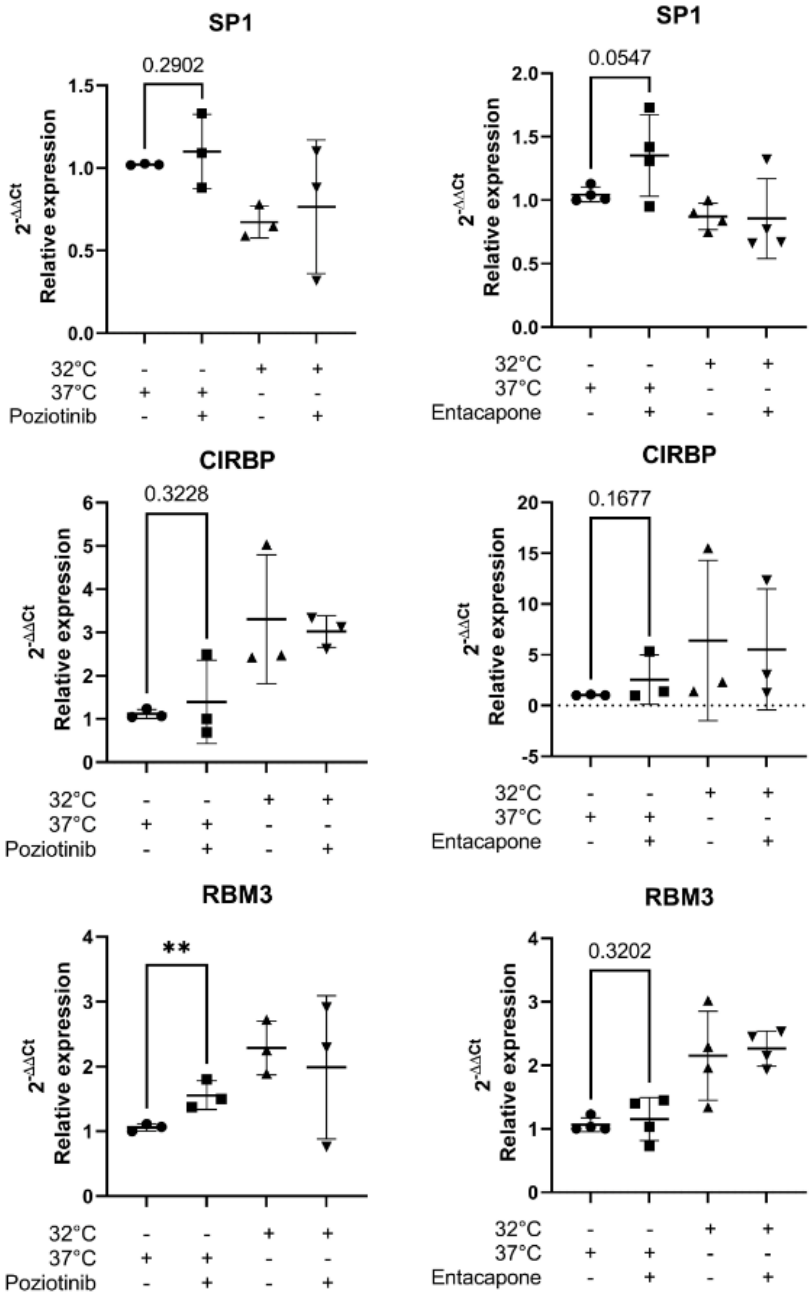

Figure S7: Expression of endogenous loci after exposure to Entacapone and Poziotinib. Relative expression of *SP1* (top), *CIRBP* (middle), *RBM3* (bottom) when compared to GAPDH after 16 h at 32°C or 37°C with and without Entacapone (left) or Poziotinib (right). Shown are data points, each data point is a biological replicate (mean of technical replicates), mean and SD where applicable. Significance levels were calculated with unpaired one tailed Student t test in GraphPad Prism. * = P<0.05, ** = P<0.01, *** = P<0.001, **** = P<0.0001.

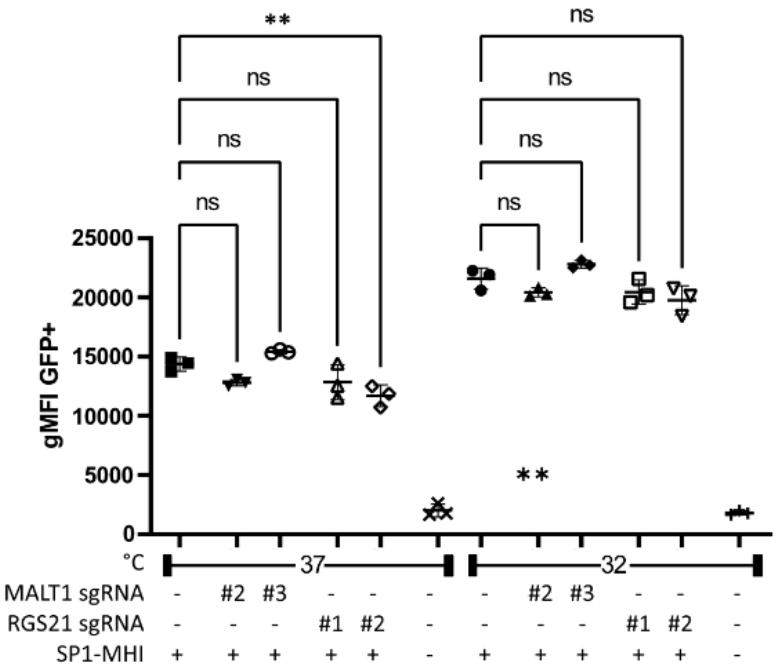

874

875 **Figure S8: *RGS21* and *MALT1* knockout did not show any significant fluorescent change.** sgRNA KO
876 for *MALT1* and *RGS21* did not show any changes in fluorescence of HEK293 cells with SP1-MHI,
877 suggesting that *MALT1* and *RGS21* do not have an impact on SP1-MHI. Shown are data points, each
878 data point is a technical replicate, mean and SD where applicable. Significance levels were calculated
879 with Šidák's multiple comparison in GraphPad Prism. * = P<0.05, ** = P<0.01, *** = P<0.001, **** =
880 P<0.0001.

881

882

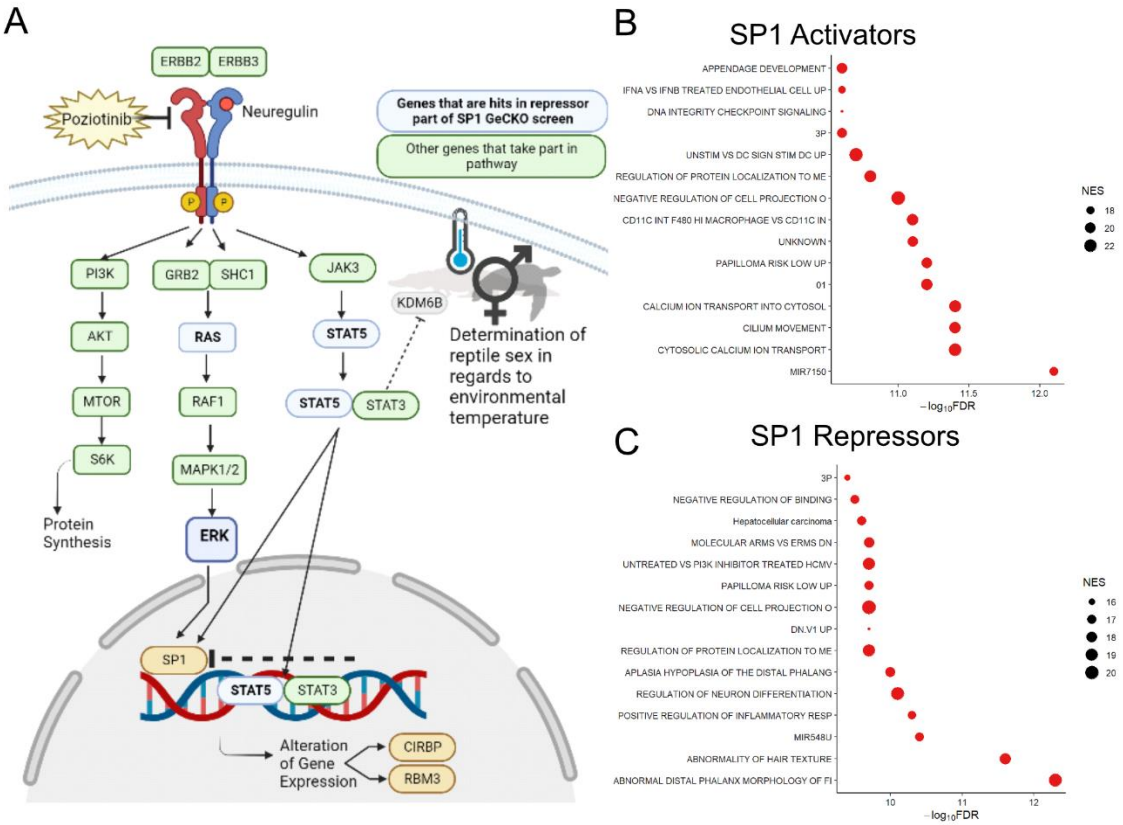

Figure S9. Pathway analysis using genes from forward mutagenesis. (A) Schematic depiction of repressors identified from both screens which land on the Neuregulin pathway. (B-C) Unbiased MSigDB pathway enrichment of highly ranked (FDR<0.25 and -Log10(RRA) >0.5) genes from the SP1 activator and SP1 repressor lists, respectively.

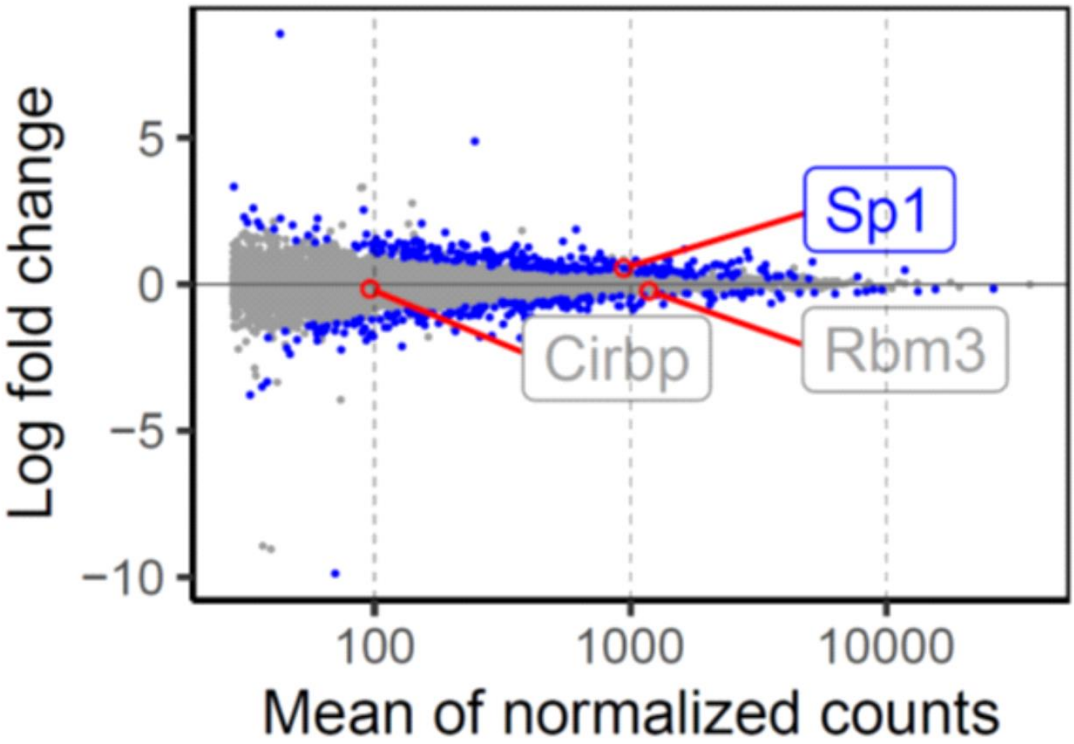

889

890 **Figure S10. *Cirbp* has fewer normalized counts compared to *Sp1* and *Rbm3.*** Normalized counts from
891 RNAseq in mESc (referring to data from **Figure 4C**).

892

893

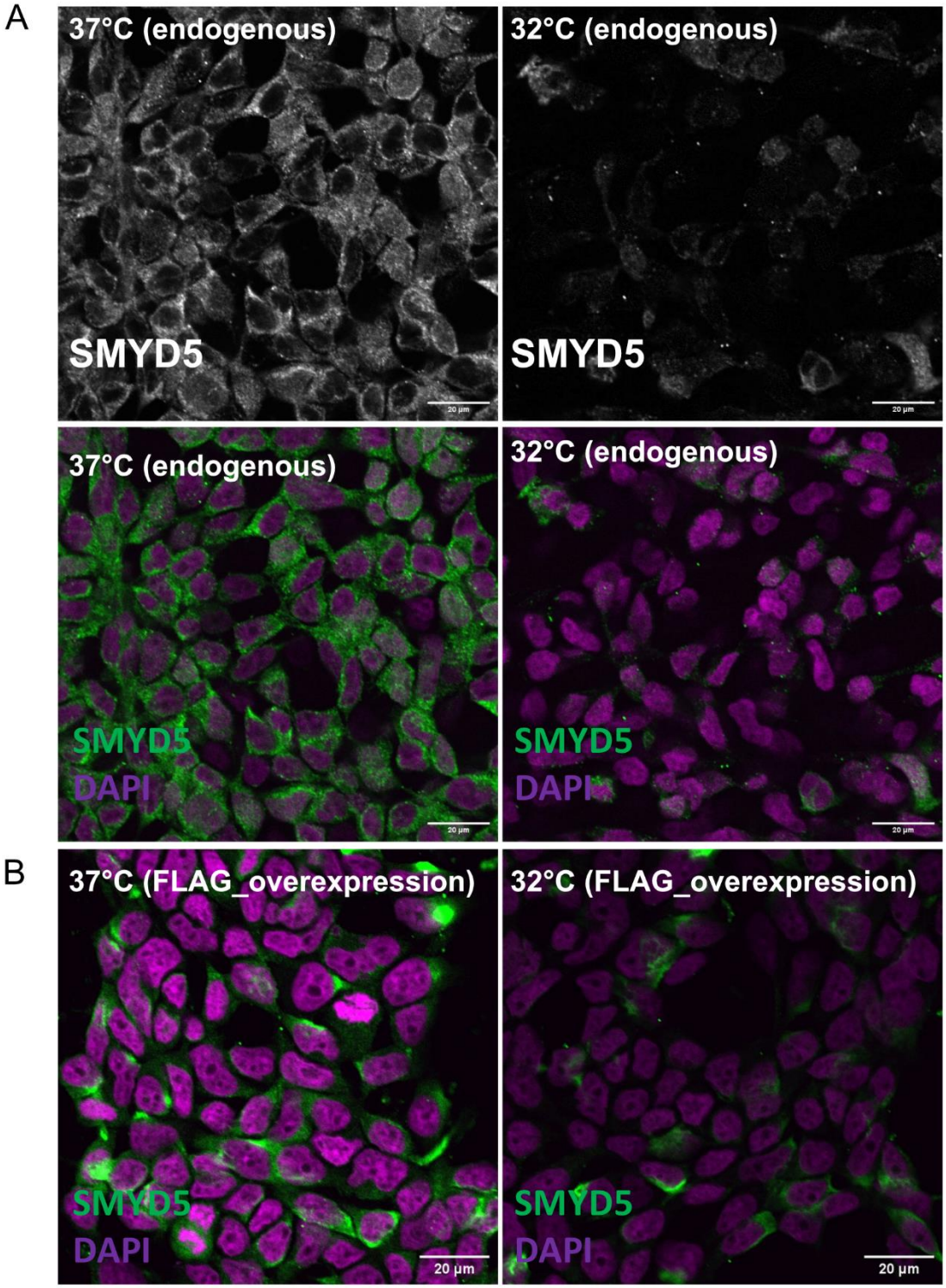

894

895 **Figure S11. Validation of temperature dependence of SMYD5.** (A) An independent biological
896 replicate with anti-SMYD5 antibody showing striking differences between two temperatures. Green
897 or white (SMYD5), purple (DAPI). (B) A validation with anti-FLAG antibody, showing same difference.
898 Green (SMYD5), purple (DAPI).

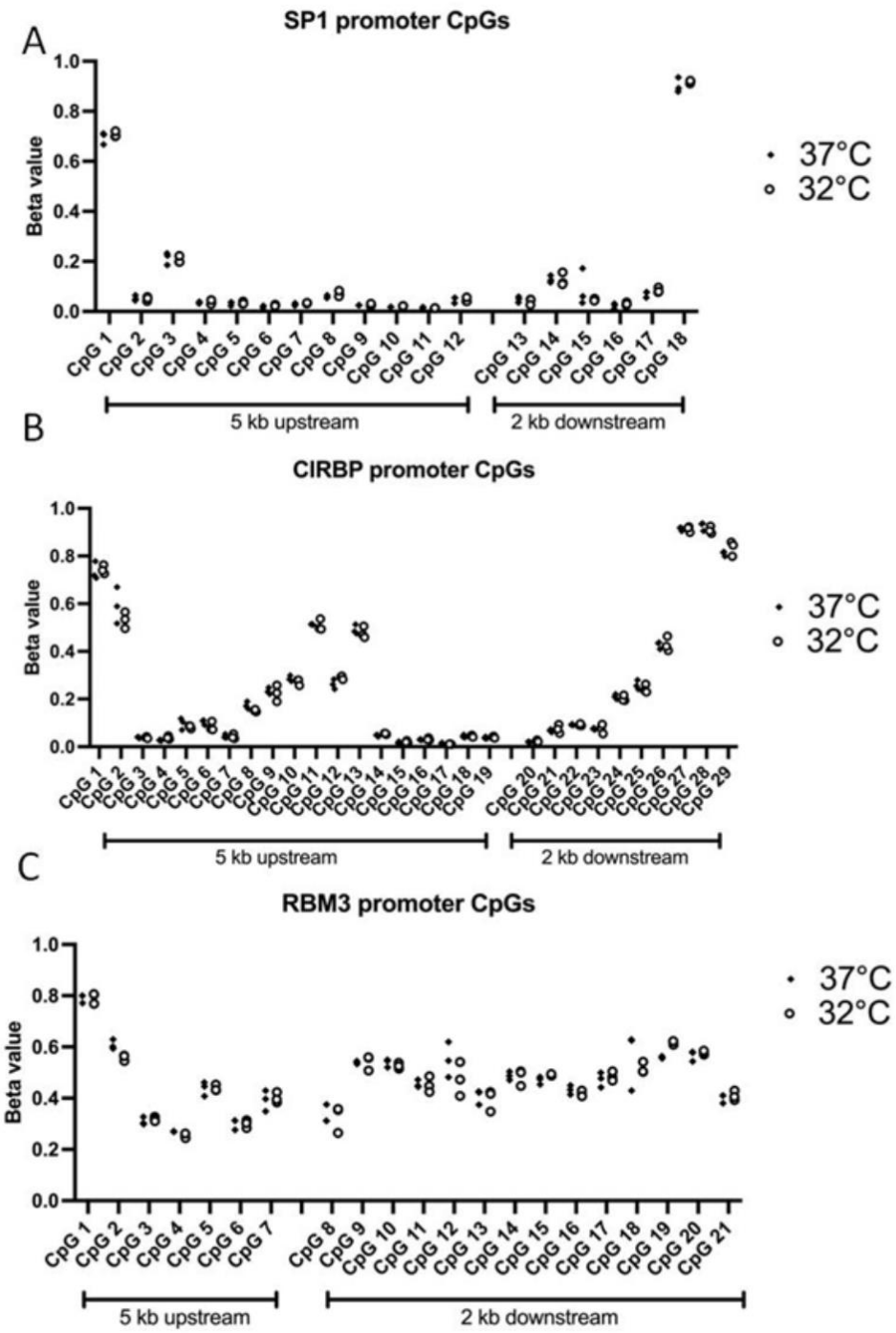

Figure S12. DNAm status at SP1, CIRBP and RBM3 promoters. (A) DNAm status of CpG dinucleotides from Illumina EPIC array 5 kb upstream and 2 kb downstream of *SP1* gene. (B) DNAm status of CpG dinucleotides from Illumina EPIC array 5 kb upstream and 2 kb downstream of *CIRBP* gene. (C) DNAm status of CpG dinucleotides from Illumina EPIC array 5 kb upstream and 2 kb downstream of *RBM3* gene.

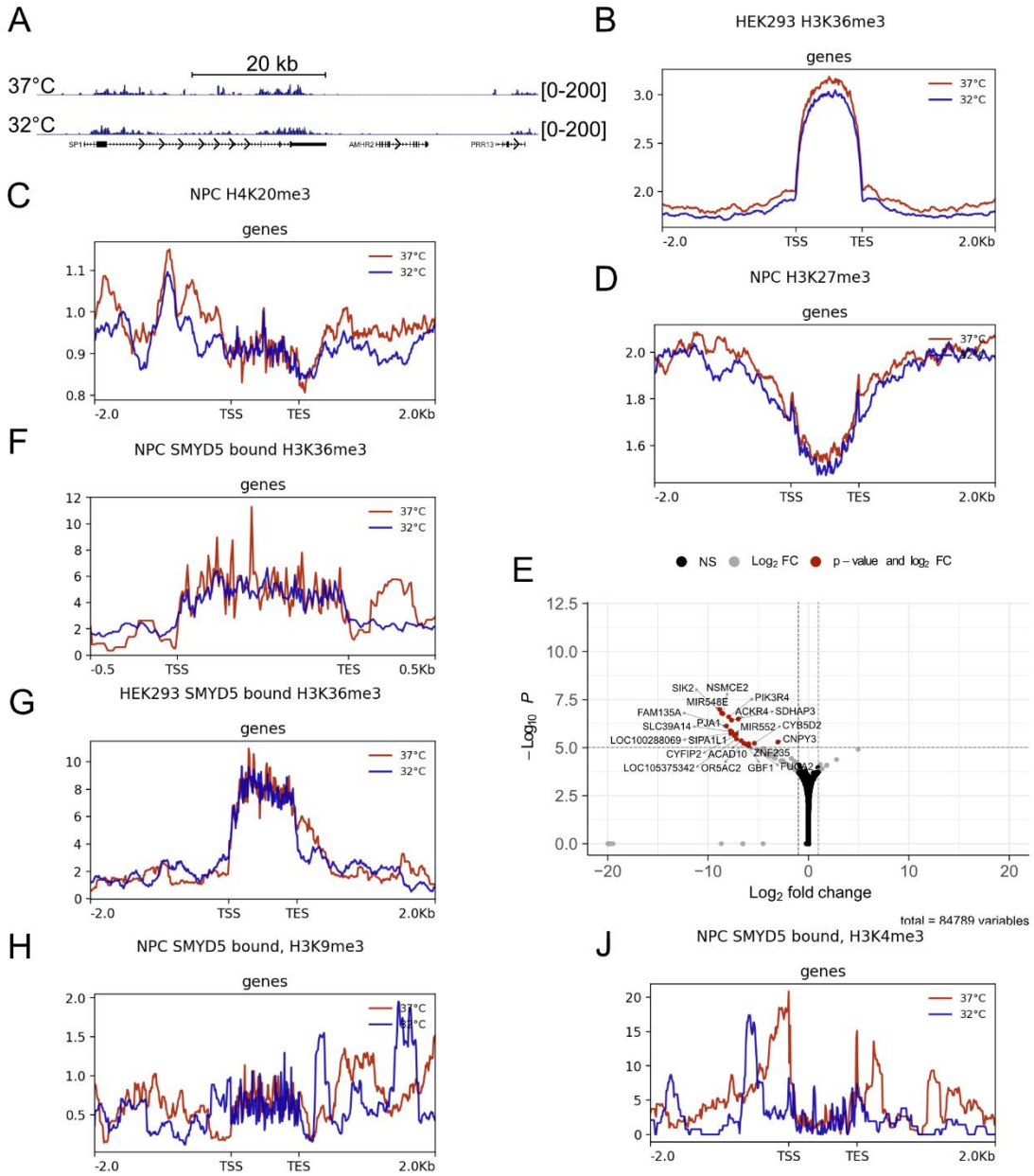

Figure S13. Methylation modification levels in NPCs and HEK293 cells. (A) H3K36me3 levels at 32°C and 37°C at *SP1* promoter in HEK293 cells. (B) Global H3K36me3 levels (all genes) in HEK293 cells. (C-D) Global H3K27me3, H4K20me3 levels, respectively (all genes) in NPCs (E) Similarly, at the gene-specific levels there is a number of genes, that have more or less H3K36me3 at 32°C compared to 37°C in HEK293 cells. Red circles indicate genes that have Log_2 fold change over 1 and p-value less than 10^{-6}, gray circles indicate Log_2 fold change over 1 but non-significant p-value and black circles indicate non-significant genes. (F-G) H3K36me3 levels at SMYD5-bound genes identified to be DEGS at the two temperatures in NPC and HEK293 cells, respectively. (H-J) H3K9me3 and H3K4me3, respectively, levels at SMYD5-bound genes identified to be DEGS at the two temperatures in NPCs.

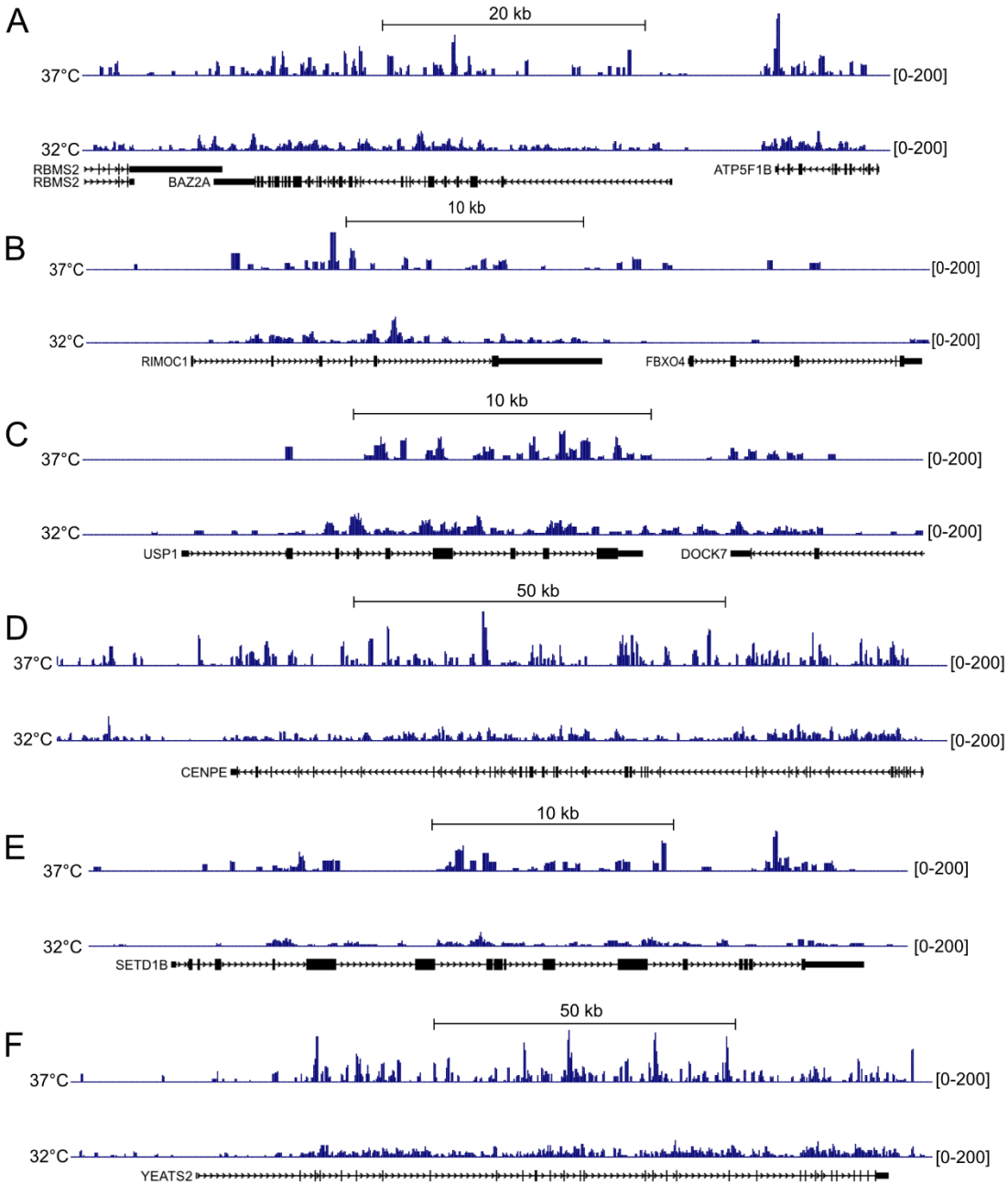

Figure S14: H3K36me3 levels on representative peaks showing differential binding at 32°C when compared to 37°C. (A-C) Increased H3K36me3 is observed for *BAZ2A*, *RIMOC1 and USP1I,* respectively, at 32°C compared to 37°C. (D-E) Decreased H3K36me3 is observed for *CENPE*, *SETD1B* and *YEATS2I,* respectively, at 37°C compared to 32°C.

928 **References**

929 1. Osilla, E. V., Marsidi, J.L., and Sharma, S. (2022). Physiology, Temperature Regulation
930 (StatPearls Publishing).

931 2. Turbill, C., Bieber, C., and Ruf, T. (2011). Hibernation is associated with increased survival and
932 the evolution of slow life histories among mammals. Proceedings of the Royal Society B:
933 Biological Sciences *278*, 3355–3363. 10.1098/RSPB.2011.0190.

934 3. Mathew, J.L., Kaur, N., and Dsouza, J.M. (2022). Therapeutic hypothermia in neonatal hypoxic
935 encephalopathy: A systematic review and meta-analysis. J Glob Health *12*.
936 10.7189/JOGH.12.04030.

937 4. Luedke, M.W., Graffagnino, C., McKinney, B.G., Piper, J., Iversen, E., and Kolls, B. (2022).
938 Association of time-temperature curves with outcomes in temperature management for
939 cardiac arrest. BMJ Neurol Open *4*. 10.1136/BMJNO-2022-000273.

940 5. Dietrichs, E.S., and Dietrichs, E. (2015). Neuroprotective effects of hypothermia. Tidsskr Nor
941 Laegeforen *135*, 1646–1651. 10.4045/tidsskr.14.1250.

942 6. Sun, Y.J., Zhang, Z.Y., Fan, B., and Li, G.Y. (2019). Neuroprotection by Therapeutic
943 Hypothermia. Front Neurosci *13*. 10.3389/FNINS.2019.00586.

944 7. Fujita, J. (1999). Cold shock response in mammalian cells. J Mol Microbiol Biotechnol *1*, 243–
945 255.

946 8. Zhu, X., Bührer, C., and Wellmann, S. (2016). Cold-inducible proteins CIRP and RBM3, a unique
947 couple with activities far beyond the cold. Cellular and Molecular Life Sciences, 1–21.
948 10.1007/s00018-016-2253-7.

949 9. Ryu, H., Lee, J., Olofsson, B.A., Mwidau, A., Deodoglu, A., Escudero, M., Flemington, E.,
950 Azizkhan-Clifford, J., Ferrante, R.J., and Ratan, R.R. (2003). Histone deacetylase inhibitors
951 prevent oxidative neuronal death independent of expanded polyglutamine repeats via an Sp1-
952 dependent pathway. Proc Natl Acad Sci U S A *100*, 4281–4286. 10.1073/PNAS.0737363100.

953 10. Yang, H.J., Zhuang, R.J., Li, Y.B., Li, T., Yuan, X., Lei, B.B., Xie, Y.F., and Wang, M. (2019). Cold-
954 inducible protein RBM3 mediates hypothermic neuroprotection against neurotoxin rotenone
955 via inhibition on MAPK signalling. J Cell Mol Med *23*, 7010–7020. 10.1111/JCMM.14588.

956 11. Bastide, A., Peretti, D., Knight, J.R.P., Grosso, S., Spriggs, R. V., Pichon, X., Sbarrato, T., Roobol,
957 A., Roobol, J., Vito, D., et al. (2017). RTN3 Is a Novel Cold-Induced Protein and Mediates
958 Neuroprotective Effects of RBM3. Current Biology *27*, 638. 10.1016/J.CUB.2017.01.047.

959 12. Chip, S., Zelmer, A., Ogunshola, O.O., Felderhoff-Mueser, U., Nitsch, C., Bührer, C., and
960 Wellmann, S. (2011). The RNA-binding protein RBM3 is involved in hypothermia induced
961 neuroprotection. Neurobiol Dis *43*, 388–396. 10.1016/j.nbd.2011.04.010.

962 13. Peretti, D., Bastide, A., Radford, H., Verity, N., Molloy, C., Martin, M.G., Moreno, J.A., Steinert,
963 J.R., Smith, T., Dinsdale, D., et al. (2015). RBM3 mediates structural plasticity and protective

964 effects of cooling in neurodegeneration. Nature 2015 518:7538 *518*, 236–239.
965 10.1038/nature14142.

966 14. Wierstra, I. (2008). Sp1: Emerging roles—Beyond constitutive activation of TATA-less
967 housekeeping genes. Biochem Biophys Res Commun *372*, 1–13. 10.1016/J.BBRC.2008.03.074.

968 15. Sumitomo, Y., Higashitsuji, H., Higashitsuji, H., Liu, Y., Fujita, T., Sakurai, T., Candeias, M.M.,
969 Itoh, K., Chiba, T., and Fujita, J. (2012). Identification of a novel enhancer that binds Sp1 and
970 contributes to induction of cold-inducible RNA-binding protein (cirp) expression in
971 mammalian cells. BMC Biotechnol *12*, 72. 10.1186/1472-6750-12-72.

972 16. Gomez-Pastor, R., Burchfiel, E.T., and Thiele, D.J. (2018). Regulation of heat shock
973 transcription factors and their roles in physiology and disease. Nat Rev Mol Cell Biol *19*, 4–19.
974 10.1038/NRM.2017.73.

975 17. Sanjana, N.E., Shalem, O., and Zhang, F. Improved vectors and genome - wide libraries for
976 CRISPR screening.

977 18. Shalem, O., Sanjana, N.E., Hartenian, E., Shi, X., Scott, D.A., Mikkelson, T., Heckl, D., Ebert, B.L.,
978 Root, D.E., Doench, J.G., et al. (2014). Genome-scale CRISPR-Cas9 knockout screening in
979 human cells. Science *343*, 84–87. 10.1126/science.1247005.

980 19. Joung, J., Konermann, S., Gootenberg, J.S., Abudayyeh, O.O., Platt, R.J., Brigham, M.D.,
981 Sanjana, N.E., and Zhang, F. (2017). Genome-scale CRISPR-Cas9 knockout and transcriptional
982 activation screening. Nat Protoc *12*, 828–863. 10.1038/nprot.2017.016.

983 20. McIntyre, S., Nelson, K.B., Mulkey, S.B., Lechpammer, M., Molloy, E., and Badawi, N. (2021).
984 Neonatal encephalopathy: Focus on epidemiology and underexplored aspects of etiology.
985 Semin Fetal Neonatal Med *26*. 10.1016/J.SINY.2021.101265.

986 21. Geneva, I.I., Cuzzo, B., Fazili, T., and Javaid, W. (2019). Normal Body Temperature: A
987 Systematic Review. Open Forum Infect Dis *6*. 10.1093/OFID/OFZ032.

988 22. Knight, J.R.P., Bastide, A., Roobol, A., Roobol, J., Jackson, T.J., Utami, W., Barrett, D.A., Smales,
989 C.M., and Willis, A.E. (2015). Eukaryotic elongation factor 2 kinase regulates the cold stress
990 response by slowing translation elongation. Biochem J *465*, 227–238. 10.1042/BJ20141014.

991 23. Shaw, G., Morse, S., Ararat, M., and Graham, F.L. (2002). Preferential transformation of
992 human neuronal cells by human adenoviruses and the origin of HEK 293 cells. The FASEB
993 Journal. 10.1096/fj.01-0995fje.

994 24. Barnes, E.N., Biedler, J.L., Spengler, B.A., and Lyser, K.M. (1981). The fine structure of
995 continuous human neuroblastoma lines SK-N-SH, SK-N-BE(2), and SK-N-MC. In Vitro *17*, 619–
996 631. 10.1007/BF02618461.

997 25. Stepanenko, A.A., and Dmitrenko, V. V (2015). HEK293 in cell biology and cancer research:
998 phenotype, karyotype, tumorigenicity, and stress-induced genome-phenotype evolution.
999 Gene *569*, 182–190. 10.1016/j.gene.2015.05.065.

1000 26. Jackson, T.C., Manole, M.D., Kotermanski, S.E., Jackson, E.K., Clark, R.S.B., and Kochanek, P.M.
1001 (2015). Cold stress protein RBM3 responds to temperature change in an ultra-sensitive
1002 manner in young neurons. Neuroscience *305*, 268–278. 10.1016/j.neuroscience.2015.08.012.

1003 27. Hartmann, J., Haap, M., Kopp, H.-G., and Lipp, H.-P. (2009). Tyrosine kinase inhibitors - a
1004 review on pharmacology, metabolism and side effects. Curr Drug Metab *10*, 470–481.
1005 10.2174/138920009788897975.

1006 28. Nelson, V., Ziehr, J., Agulnik, M., and Johnson, M. (2013). Afatinib: emerging next-generation
1007 tyrosine kinase inhibitor for NSCLC. Onco Targets Ther *6*, 135–143. 10.2147/OTT.S23165.

1008 29. Kim, T.M., Lee, K.W., Oh, D.Y., Lee, J.S., Im, S.A., Kim, D.W., Han, S.W., Kim, Y.J., Kim, T.Y., Kim,
1009 J.H., et al. (2018). Phase 1 Studies of Poziotinib, an Irreversible Pan-HER Tyrosine Kinase
1010 Inhibitor in Patients with Advanced Solid Tumors. Cancer Res Treat *50*, 835–842.
1011 10.4143/CRT.2017.303.

1012 30. Erber, R., Thurnher, A., Katsen, A.D., Groth, G., Kerger, H., Hammes, H.P., Menger, M.D.,
1013 Ullrich, A., and Vajkoczy, P. (2004). Combined inhibition of VEGF and PDGF signaling enforces
1014 tumor vessel regression by interfering with pericyte-mediated endothelial cell survival
1015 mechanisms. FASEB J *18*, 338–340. 10.1096/FJ.03-0271FJE.

1016 31. Lee, H., Kim, J.W., Choi, D.K., Yu, J.H., Kim, J.H., Lee, D.S., and Min, S.H. (2020). Poziotinib
1017 suppresses ovarian cancer stem cell growth via inhibition of HER4-mediated STAT5 pathway.
1018 Biochem Biophys Res Commun *526*, 158–164. 10.1016/J.BBRC.2020.03.046.

1019 32. Grinstein, E., Jundt, F., Weinert, I., Wernet, P., and Royer, H.D. (2002). Sp1 as G1 cell cycle
1020 phase specific transcription factor in epithelial cells. Oncogene 2002 21:10 *21*, 1485–1492.
1021 10.1038/sj.onc.1205211.

1022 33. Li, W., Xu, H., Xiao, T., Cong, L., Love, M.I., Zhang, F., Irizarry, R.A., Liu, J.S., Brown, M., and Liu,
1023 X.S. (2014). MAGeCK enables robust identification of essential genes from genome-scale
1024 CRISPR/Cas9 knockout screens. Genome Biol *15*, 554. 10.1186/s13059-014-0554-4.

1025 34. Hsu, P.D., Lander, E.S., and Zhang, F. (2014). Development and Applications of CRISPR-Cas9 for
1026 Genome Engineering. Cell *157*, 1262–1278. 10.1016/j.cell.2014.05.010.

1027 35. Nagai, G., and Nakaoka, Y. (1998). Cooling sensitive [Ca2+](i) response associated with
1028 signaling of G protein-coupled receptors. Biochem Biophys Res Commun *248*, 733–737.
1029 10.1006/BBRC.1998.8873.

1030 36. Chelban, V., Patel, N., Vandrovcova, J., Zanetti, M.N., Lynch, D.S., Ryten, M., Botía, J.A., Bello,
1031 O., Tribollet, E., Efthymiou, S., et al. (2017). Mutations in NKX6-2 Cause Progressive Spastic
1032 Ataxia and Hypomyelination. Am J Hum Genet *100*, 969–977. 10.1016/J.AJHG.2017.05.009.

1033 37. ZNF260 zinc finger protein 260 [Homo sapiens (human)] - Gene - NCBI
1034 https://www.ncbi.nlm.nih.gov/gene?Db=gene&Cmd=DetailsSearch&Term=339324#gene-
1035 expression.

1036 38. Burke, T.L., and Grant, P.A. (2009). Histone Acetylation Complexes. Handbook of Cell
1037 Signaling, Second Edition *3*, 2369–2378. 10.1016/B978-0-12-374145-5.00285-0.

1038 39. Zhou, X., Shang, Y.N., Lu, R., Fan, C.W., and Mo, X.M. (2019). High ANKZF1 expression is
1039 associated with poor overall survival and recurrence-free survival in colon cancer.
1040 https://doi.org/10.2217/fon-2018-0920 *15*, 2093–2106. 10.2217/FON-2018-0920.

1041 40. Tawamie, H., Martianov, I., Wohlfahrt, N., Buchert, R., Mengus, G., Uebe, S., Janiri, L., Hirsch,
1042 F.W., Schumacher, J., Ferrazzi, F., et al. (2017). Hypomorphic Pathogenic Variants in TAF13 Are
1043 Associated with Autosomal-Recessive Intellectual Disability and Microcephaly. Am J Hum
1044 Genet *100*, 555. 10.1016/J.AJHG.2017.01.032.

1045 41. ZNF71 zinc finger protein 71 [Homo sapiens (human)] - Gene - NCBI
1046 https://www.ncbi.nlm.nih.gov/gene?Db=gene&Cmd=DetailsSearch&Term=58491.

1047 42. Yu, H. V., Tao, L., Llamas, J., Wang, X., Nguyen, J.D., Trecek, T., and Segil, N. (2021). POU4F3
1048 pioneer activity enables ATOH1 to drive diverse mechanoreceptor differentiation through a
1049 feed-forward epigenetic mechanism. Proc Natl Acad Sci U S A *118*.
1050 10.1073/PNAS.2105137118/-/DCSUPPLEMENTAL.

1051 43. GATAD2A GATA zinc finger domain containing 2A [Homo sapiens (human)] - Gene - NCBI
1052 https://www.ncbi.nlm.nih.gov/gene/54815.

1053 44. Zhang, Y., Fang, Y., Tang, Y., Han, S., Jia, J., Wan, X., Chen, J., Yuan, Y., Zhao, B., and Fang, D.
1054 (2022). SMYD5 catalyzes histone H3 lysine 36 trimethylation at promoters. Nature
1055 Communications 2022 13:1 *13*, 1–19. 10.1038/s41467-022-30940-1.

1056 45. Kidder, B.L., He, R., Wangsa, D., Padilla-Nash, H.M., Bernardo, M.M., Sheng, S., Ried, T., and
1057 Zhao, K. (2017). SMYD5 Controls Heterochromatin and Chromosome Integrity during
1058 Embryonic Stem Cell Differentiation. Cancer Res *77*, 6729–6745. 10.1158/0008-5472.CAN-17-
1059 0828.

1060 46. Murphy, M.W., Sarver, A.L., Rice, D., Hatzi, K., Ye, K., Melnick, A., Heckert, L.L., Zarkower, D.,
1061 and Bardwell, V.J. (2010). Genome-wide analysis of DNA binding and transcriptional
1062 regulation by the mammalian Doublesex homolog DMRT1 in the juvenile testis. Proc Natl
1063 Acad Sci U S A *107*, 13360–13365. 10.1073/PNAS.1006243107/SUPPL_FILE/SD01.XLS.

1064 47. Weber, C., Zhou, Y., Lee, J.G., Looger, L.L., Qian, G., Ge, C., and Capel, B. (2020). Temperature-
1065 dependent sex determination is mediated by pSTAT3 repression of Kdm6b. Science (1979)
1066 *368*, 303–306. 10.1126/SCIENCE.AAZ4165/SUPPL_FILE/AAZ4165_S1.MP4.

1067 48. Kim, D.H., Doyle, M.R., Sung, S., and Amasino, R.M. (2009). Vernalization: winter and the
1068 timing of flowering in plants. Annu Rev Cell Dev Biol *25*, 277–299.
1069 10.1146/annurev.cellbio.042308.113411.

1070 49. Fellous, A., Earley, R.L., and Silvestre, F. (2019). The Kdm/Kmt gene families in the self-
1071 fertilizing mangrove rivulus fish, Kryptolebias marmoratus, suggest involvement of histone
1072 methylation machinery in development and reproduction. Gene *687*, 173–187.
1073 10.1016/J.GENE.2018.11.046.

1074 50. Youn, J.Y., Dyakov, B.J.A., Zhang, J., Knight, J.D.R., Vernon, R.M., Forman-Kay, J.D., and
1075 Gingras, A.C. (2019). Properties of Stress Granule and P-Body Proteomes. Mol Cell *76*, 286–
1076 294. 10.1016/J.MOLCEL.2019.09.014.

1077 51. Aljazi, M.B., Gao, Y., Wu, Y., and He, J. (2022). SMYD5 is a histone H3-specific
1078 methyltransferase mediating mono-methylation of histone H3 lysine 36 and 37. Biochem
1079 Biophys Res Commun *599*, 142–147. 10.1016/J.BBRC.2022.02.043.

1080 52. Diaz, J., Abiola, S., Kim, N., Avaritt, O., Flock, D., Yu, J., Northington, F.J., and Chavez-Valdez, R.
1081 (2017). Therapeutic hypothermia provides variable protection against behavioral deficits after
1082 neonatal HI: A potential role for BDNF. Dev Neurosci *39*, 257. 10.1159/000454949.

1083 53. Xi, Y., Park, S.R., Kim, D.H., Kim, E.D., and Sung, S. (2020). Transcriptome and epigenome
1084 analyses of vernalization in Arabidopsis thaliana. Plant J *103*, 1490. 10.1111/TPJ.14817.

1085 54. Fan, L., Lesser, A.F., Sweet, D.R., Keerthy, K.S., Lu, Y., Chan, E.R., Vinayachandran, V., Ilkayeva,
1086 O., Das, T., Newgard, C.B., et al. (2022). KLF15 controls brown adipose tissue transcriptional
1087 flexibility and metabolism in response to various energetic demands. iScience *25*, 105292.
1088 10.1016/J.ISCI.2022.105292.

1089 55. Katano-Toki, A., Satoh, T., Tomaru, T., Yoshino, S., Ishizuka, T., Ishii, S., Ozawa, A., Shibusawa,
1090 N., Tsuchiya, T., Saito, T., et al. (2013). THRAP3 Interacts with HELZ2 and Plays a Novel Role in
1091 Adipocyte Differentiation. Molecular Endocrinology *27*, 769. 10.1210/ME.2012-1332.

1092 56. THRAP3 thyroid hormone receptor associated protein 3 [Homo sapiens (human)] - Gene -
1093 NCBI https://www.ncbi.nlm.nih.gov/gene?Db=gene&Cmd=DetailsSearch&Term=9967.

1094 57. Guo, K., Searfoss, G., Krolikowski, D., Pagnoni, M., Franks, C., Clark, K., Yu, K.T., Jaye, M., and
1095 Ivashchenko, Y. (2001). Hypoxia induces the expression of the pro-apoptotic gene BNIP3. Cell
1096 Death Differ *8*, 367–376. 10.1038/SJ.CDD.4400810.

1097 58. Abdel-Wahab, O., Adli, M., LaFave, L.M., Gao, J., Hricik, T., Shih, A.H., Pandey, S., Patel, J.P.,
1098 Chung, Y.R., Koche, R., et al. (2012). ASXL1 mutations promote myeloid transformation
1099 through loss of PRC2-mediated gene repression. Cancer Cell *22*, 180–193.
1100 10.1016/J.CCR.2012.06.032.

1101 59. Kaakkola, S. (2000). Clinical pharmacology, therapeutic use and potential of COMT inhibitors
1102 in Parkinson's disease. Drugs *59*, 1233–1250. 10.2165/00003495-200059060-00004.

1103 60. Feng, Z., Saha, L., Dritsa, C., Wan, Q., and Glebov, O.O. (2022). Temperature-dependent
1104 structural plasticity of hippocampal synapses. Front Cell Neurosci *16*, 520.
1105 10.3389/FNCEL.2022.1009970/BIBTEX.

1106 61. Carvelli, L., Blakely, R.D., and DeFelice, L.J. (2008). Dopamine transporter/syntaxin 1A
1107 interactions regulate transporter channel activity and dopaminergic synaptic transmission.
1108 Proc Natl Acad Sci U S A *105*, 14192–14197. 10.1073/PNAS.0802214105.

1109 62. Gao, H., Chakraborty, G., Lee-Lim, A.P., Mavrakis, K.J., Wendel, H.G., and Giancotti, F.G.
1110 (2014). Forward genetic screens in mice uncover mediators and suppressors of metastatic

1111 reactivation. Proc Natl Acad Sci U S A *111*, 16532–16537.
1112 10.1073/PNAS.1403234111/SUPPL_FILE/PNAS.201403234SI.PDF.

1113 63. INDACOCHEA, A., GUERRERO, S., UREÑA, M., ARAUJO, F., COLL, O., LLEONART, M.E., and
1114 GEBAUER, F. (2021). Cold-inducible RNA binding protein promotes breast cancer cell
1115 malignancy by regulating Cystatin C levels. RNA *27*, 190–201. 10.1261/RNA.076422.120.

1116 64. Nicolas, M., Noe, V., Jensen, K., and Ciudad CJ (2001). Cloning and characterization of the 5'-
1117 flanking region of the human transcription factor Sp1 gene. . J Biol Chem, 22126-22132.

1118 65. Yang, F., Eckardt, S., Leu, N.A., McLaughlin, K.J., and Wang, P.J. (2008). Mouse TEX15 is
1119 essential for DNA double-strand break repair and chromosomal synapsis during male meiosis.
1120 J Cell Biol *180*, 673. 10.1083/JCB.200709057.

1121 66. TEX15 testis expressed 15, meiosis and synapsis associated [Homo sapiens (human)] - Gene -
1122 NCBI https://www.ncbi.nlm.nih.gov/gene/56154.

1123 67. Hanna, C.W., Huang, J., Belton, C., Reinhardt, S., Dahl, A., Andrews, S., Francis Stewart, A.,
1124 Kranz, A., and Kelsey, G. (2022). Loss of histone methyltransferase SETD1B in oogenesis
1125 results in the redistribution of genomic histone 3 lysine 4 trimethylation. Nucleic Acids Res *50*,
1126 1993. 10.1093/NAR/GKAC051.

1127 68. Pajoro, A., Severing, E., Angenent, G.C., and Immink, R.G.H. (2017). Histone H3 lysine 36
1128 methylation affects temperature-induced alternative splicing and flowering in plants. Genome
1129 Biol *18*, 1–12. 10.1186/S13059-017-1235-X/FIGURES/4.

1130 69. Michaels, K.K., Mostafa, S.M., Capella, J.R., and Moore, C.L. (2020). Regulation of alternative
1131 polyadenylation in the yeast Saccharomyces cerevisiae by histone H3K4 and H3K36
1132 methyltransferases. Nucleic Acids Res *48*, 5407–5425. 10.1093/NAR/GKAA292.

1133 70. Xu, S.J., Lombroso, S.I., Fischer, D.K., Carpenter, M.D., Marchione, D.M., Hamilton, P.J., Lim,
1134 C.J., Neve, R.L., Garcia, B.A., Wimmer, M.E., et al. (2021). Chromatin-mediated alternative
1135 splicing regulates cocaine-reward behavior. Neuron *109*, 2943-2966.e8.
1136 10.1016/J.NEURON.2021.08.008.

1137 71. Preußner, M., Goldammer, G., Neumann, A., Haltenhof, T., Rautenstrauch, P., Müller-
1138 McNicoll, M., and Heyd, F. (2017). Body Temperature Cycles Control Rhythmic Alternative
1139 Splicing in Mammals. Mol Cell *67*, 433-446.e4. 10.1016/J.MOLCEL.2017.06.006.

1140 72. Horii, Y., Shiina, T., Uehara, S., Nomura, K., Shimaoka, H., Horii, K., and Shimizu, Y. (2019).
1141 Hypothermia induces changes in the alternative splicing pattern of cold-inducible RNA-binding
1142 protein transcripts in a non-hibernator, the mouse. Biomed Res *40*, 153–161.
1143 10.2220/BIOMEDRES.40.153.

1144 73. Sano, Y., Shiina, T., Naitou, K., Nakamori, H., and Shimizu, Y. (2015). Hibernation-specific
1145 alternative splicing of the mRNA encoding cold-inducible RNA-binding protein in the hearts of
1146 hamsters. Biochem Biophys Res Commun *462*, 322–325. 10.1016/j.bbrc.2015.04.135.

1147 74. Smart, F., Aschrafi, A., Atkins, A., Owens, G.C., Pilotte, J., Cunningham, B.A., and Vanderklish,
1148 P.W. (2007). Two isoforms of the cold-inducible mRNA-binding protein RBM3 localize to
1149 dendrites and promote translation. J Neurochem *101*, 1367–1379. 10.1111/J.1471-
1150 4159.2007.04521.X.

1151 75. Al-Fageeh, M.B., and Smales, C.M. (2013). Alternative promoters regulate cold inducible RNA-
1152 binding (CIRP) gene expression and enhance transgene expression in mammalian cells. Mol
1153 Biotechnol *54*, 238–249. 10.1007/s12033-013-9649-5.

1154 76. Nicolas, M., Noe, V., Jensen, K.B., and Ciudad, C.J. (2001). Cloning and characterization of the
1155 5'-flanking region of the human transcription factor Sp1 gene. J Biol Chem *276*, 22126–22132.
1156 10.1074/jbc.M010740200.

1157 77. Chambers, S.M., Fasano, C.A., Papapetrou, E.P., Tomishima, M., Sadelain, M., Studer, L., and
1158 Author, N.B. (2009). Highly efficient neural conversion of human ES and iPS cells by dual
1159 inhibition of SMAD signaling HHS Public Access Author manuscript. Nat Biotechnol *27*, 275–
1160 280. 10.1038/nbt.1529.

1161 78. Xiang, J., Wan, C., Guo, R., and Guo, D. (2016). Is Hydrogen Peroxide a Suitable Apoptosis
1162 Inducer for All Cell Types? Biomed Res Int *2016*. 10.1155/2016/7343965.

1163 79. Kutner, R.H., Zhang, X.Y., and Reiser, J. (2009). Production, concentration and titration of
1164 pseudotyped HIV-1-based lentiviral vectors. Nat Protoc *4*, 495–505. 10.1038/nprot.2009.22.

1165 80. Wang, B., Wang, M., Zhang, W., Xiao, T., Chen, C.H., Wu, A., Wu, F., Traugh, N., Wang, X., Li,
1166 Z., et al. (2019). Integrative analysis of pooled CRISPR genetic screens using MAGeCKFlute. Nat
1167 Protoc *14*, 756–780. 10.1038/s41596-018-0113-7.

1168 81. Statistical R Core Team (2017). R Foundation for Statistical Computing Vienna Austria. R: A
1169 language and environment for computing.

1170 82. Rueden, C.T., Schindelin, J., Hiner, M.C., DeZonia, B.E., Walter, A.E., Arena, E.T., and Eliceiri,
1171 K.W. (2017). ImageJ2: ImageJ for the next generation of scientific image data. BMC
1172 Bioinformatics *18*, 1–26. 10.1186/S12859-017-1934-Z/FIGURES/7.

1173 83. Schindelin, J., Arganda-Carreras, I., Frise, E., Kaynig, V., Longair, M., Pietzsch, T., Preibisch, S.,
1174 Rueden, C., Saalfeld, S., Schmid, B., et al. (2012). Fiji: an open-source platform for biological-
1175 image analysis. Nature Methods 2012 9:7 *9*, 676–682. 10.1038/nmeth.2019.

1176 84. Stirling, D.R., Swain-Bowden, M.J., Lucas, A.M., Carpenter, A.E., Cimini, B.A., and Goodman, A.
1177 (2021). CellProfiler 4: improvements in speed, utility and usability. BMC Bioinformatics *22*.
1178 10.1186/S12859-021-04344-9.

1179 85. Fortin, J.P., Triche, T.J., and Hansen, K.D. (2017). Preprocessing, normalization and integration
1180 of the Illumina HumanMethylationEPIC array with minfi. Bioinformatics *33*, 558.
1181 10.1093/BIOINFORMATICS/BTW691.

1182 86. Triche, T.J., Weisenberger, D.J., Van Den Berg, D., Laird, P.W., and Siegmund, K.D. (2013). Low-
1183 level processing of Illumina Infinium DNA Methylation BeadArrays. Nucleic Acids Res *41*, e90.
1184 10.1093/NAR/GKT090.

1185 87. Aryee, M.J., Jaffe, A.E., Corrada-Bravo, H., Ladd-Acosta, C., Feinberg, A.P., Hansen, K.D., and
1186 Irizarry, R.A. (2014). Minfi: a flexible and comprehensive Bioconductor package for the
1187 analysis of Infinium DNA methylation microarrays. Bioinformatics *30*, 1363.
1188 10.1093/BIOINFORMATICS/BTU049.

1189 88. Leek, J.T., Johnson, W.E., Parker, H.S., Jaffe, A.E., and Storey, J.D. (2012). The sva package for
1190 removing batch effects and other unwanted variation in high-throughput experiments.
1191 Bioinformatics *28*, 882. 10.1093/BIOINFORMATICS/BTS034.

1192 89. Ritchie, M.E., Phipson, B., Wu, D., Hu, Y., Law, C.W., Shi, W., and Smyth, G.K. (2015). limma
1193 powers differential expression analyses for RNA-sequencing and microarray studies. Nucleic
1194 Acids Res *43*, e47. 10.1093/NAR/GKV007.

1195 90. Kong, N.R., Chai, L., Tenen, D.G., and Bassal, M.A. (2021). A modified CUT&RUN protocol and
1196 analysis pipeline to identify transcription factor binding sites in human cell lines. STAR Protoc
1197 *2*. 10.1016/J.XPRO.2021.100750.

1198 91. Martin, M. (2011). Cutadapt removes adapter sequences from high-throughput sequencing
1199 reads. EMBnet J *17*, 10–12. 10.14806/EJ.17.1.200.

1200 92. Langmead, B., and Salzberg, S.L. (2012). Fast gapped-read alignment with Bowtie 2. Nat
1201 Methods *9*, 357–359. 10.1038/nmeth.1923.

1202 93. Li, H., Handsaker, B., Wysoker, A., Fennell, T., Ruan, J., Homer, N., Marth, G., Abecasis, G., and
1203 Durbin, R. (2009). The Sequence Alignment/Map format and SAMtools. Bioinformatics *25*,
1204 2078–2079. 10.1093/BIOINFORMATICS/BTP352.

1205 94. Luo, Y., Hitz, B.C., Gabdank, I., Hilton, J.A., Kagda, M.S., Lam, B., Myers, Z., Sud, P., Jou, J., Lin,
1206 K., et al. (2020). New developments on the Encyclopedia of DNA Elements (ENCODE) data
1207 portal. Nucleic Acids Res *48*, D882–D889. 10.1093/NAR/GKZ1062.

1208 95. Quinlan, A.R., and Hall, I.M. (2010). BEDTools: a flexible suite of utilities for comparing
1209 genomic features. Bioinformatics *26*, 841–842. 10.1093/BIOINFORMATICS/BTQ033.

1210 96. Meers, M.P., Tenenbaum, D., and Henikoff, S. (2019). Peak calling by Sparse Enrichment
1211 Analysis for CUT&RUN chromatin profiling. Epigenetics Chromatin *12*, 1–11. 10.1186/S13072-
1212 019-0287-4/FIGURES/6.

1213 97. Stark, R., and Brown, G. (2012). DiffBind : differential binding analysis of ChIP-Seq peak data.

1214 98. Yu, G., Wang, L.G., and He, Q.Y. (2015). ChIPseeker: an R/Bioconductor package for ChIP peak
1215 annotation, comparison and visualization. Bioinformatics *31*, 2382–2383.
1216 10.1093/BIOINFORMATICS/BTV145.

1217 99. Team BC, and Maintainer BP (2019). TxDb.Hsapiens.UCSC.hg38.knownGene: Annotation
1218 package for TxDb object(s).

1219 100. Carlson M (2019). org.Hs.eg.db: Genome wide annotation for Human. .

1220 101. Ramírez, F., Dündar, F., Diehl, S., Grüning, B.A., and Manke, T. (2014). deepTools: a flexible
1221 platform for exploring deep-sequencing data. Nucleic Acids Res *42*, W187.
1222 10.1093/NAR/GKU365.

1223 102. Bernas, S.N., Leiter, O., Walker, T.L., and Kempermann, G. (2017). Isolation, Culture and
1224 Differentiation of Adult Hippocampal Precursor Cells. Bio Protoc *7*.
1225 10.21769/BIOPROTOC.2603.

1226 103. Soneson, C., Love, M.I., and Robinson, M.D. (2016). Differential analyses for RNA-seq:
1227 Transcript-level estimates improve gene-level inferences. F1000Res *4*.
1228 10.12688/F1000RESEARCH.7563.2/DOI.

1229 104. Team BC, and Maintainer BP (2016). TxDb.Mmusculus.UCSC.mm10.ensGene: Annotation
1230 package for TxDb object(s)..

1231 105. Love, M.I., Huber, W., and Anders, S. (2014). Moderated estimation of fold change and
1232 dispersion for RNA-seq data with DESeq2. Genome Biol *15*, 1–21. 10.1186/S13059-014-0550-
1233 8/FIGURES/9.

1234 106. Shen L, and Sinai ISoMaM (2022). GeneOverlap: Test and visualize gene overlaps. .

1235 107. Subramanian, A., Tamayo, P., Mootha, V.K., Mukherjee, S., Ebert, B.L., Gillette, M.A.,
1236 Paulovich, A., Pomeroy, S.L., Golub, T.R., Lander, E.S., et al. (2005). Gene set enrichment
1237 analysis: a knowledge-based approach for interpreting genome-wide expression profiles. Proc
1238 Natl Acad Sci U S A *102*, 15545–15550. 10.1073/PNAS.0506580102.

1239 108. Mootha, V.K., Lindgren, C.M., Eriksson, K.F., Subramanian, A., Sihag, S., Lehar, J., Puigserver,
1240 P., Carlsson, E., Ridderstråle, M., Laurila, E., et al. (2003). PGC-1alpha-responsive genes
1241 involved in oxidative phosphorylation are coordinately downregulated in human diabetes. Nat
1242 Genet *34*, 267–273. 10.1038/NG1180.

1243 109. Liberzon, A., Birger, C., Thorvaldsdóttir, H., Ghandi, M., Mesirov, J.P., and Tamayo, P. (2015).
1244 The Molecular Signatures Database (MSigDB) hallmark gene set collection. Cell Syst *1*, 417–
1245 425. 10.1016/J.CELS.2015.12.004.

1246

1247